Light-induced metastable defects in hydrogenated amorphous silicon: A systematic study

M. Stutzmann, W. B. Jackson, and C. C. Tsai
Xerox Palo Alto Research Center, 3333 Coyote Hill Road, Palo Alto, California 94304
(Received 14 December 1984)

We study the magnitude of metastable light-induced changes in undoped hydrogenated amorphous silicon (the Staebler-Wronski effect) with electron-spin-resonance and photoconductivity measurements. The influence of the following parameters is investigated in a systematic way: sample thickness, impurity content, illumination time, light intensity, photon energy, and illumination and annealing temperatures. The experimental results can be explained quantitatively by a model based on the nonradiative recombination of photoexcited carriers as the defect-creating step. In the framework of this model, the Staebler-Wronski effect is an intrinsic, self-limiting bulk process, characterized by a strongly sublinear dependence on the total light exposure of a sample. The experimental results suggest that the metastable changes are caused by recombination-induced breaking of weak Si—Si bonds, rather than by trapping of excess carriers in already existing defects. Hydrogen could be involved in the microscopic mechanism as a stabilizing element. The main metastable defect created by prolonged illumination is the silicon dangling bond. An analysis of the annealing behavior shows that a broad distribution of metastable dangling bonds exists, characterized by a variation of the energy barrier separating the metastable state from the stable ground state between 0.9 and 1.3 eV.

I. INTRODUCTION

The glassy or amorphous phase of a material may well be characterized by the fact that the configurational ground state is not given by an absolute and isolated minimum of the total potential energy, but rather by a more flexible arrangement of the atoms allowing configurations with different local minima of the potential energy separated by a more or less continuous distribution of potential barriers. The possibility of transitions between adjacent local potential minima in an amorphous solid leads to a number of processes which, in quality or quantity, are not commonly observed in their crystalline counterparts. To be more specific, consider a situation as shown in Fig. 1, where two minima of the total energy exist as a function of a suitably chosen configurational coordinate q. The minima differ by an energy ΔE and are separated by a potential barrier $(V_0,\Delta q)$ with $\Delta q = |q_1 - q_0|$. In this picture, the crystalline state will be characterized by the existence of relatively few, well-defined, and discrete possible values for the parameters ΔE, V_0, and Δq. In the amorphous case a continuous distribution of these quantities is possible, a fact that introduces a noticeable difference from the crystalline case: a nonzero density of atomic configurations with sufficiently small values of ΔE, V_0, and Δq, so that at any temperature tunneling transitions between the two local minima in Fig. 1 can occur in the amorphous material. This leads to a new class of structural excitations known as two-level systems (TLS) which do not exist in crystalline materials. The TLS are thought to cause a variety of low-temperature anomalies of amorphous solids.[1]

A second class of phenomena, both in crystalline and amorphous solids, is observed under non-thermal-equilibrium conditions, for example, during illumination of a semiconductor. If the externally applied excitation is $E_{ex} \geq \Delta E + V_0$, stimulated transitions between the configurational states q_0 and q_1 become possible. As a conse-

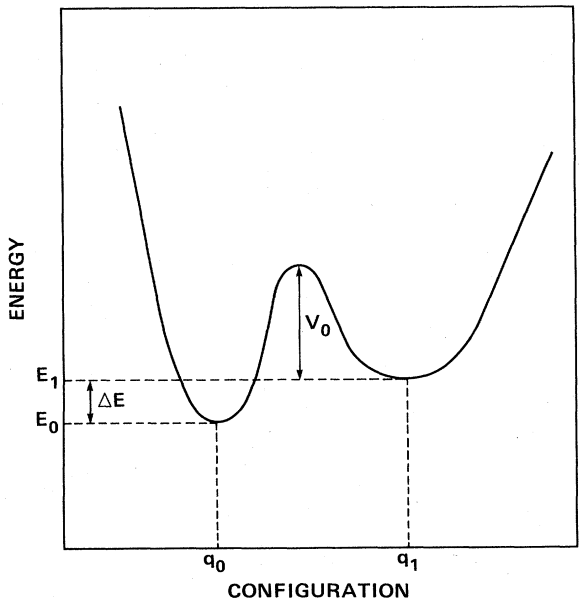

FIG. 1. Energy-configuration diagram used for a phenomenological description of the two-level systems (TLS) and metastable defects in a-Si:H. In the case of the TLS the energy barrier, V_0 and $\Delta q = |q_1 - q_0|$, is small enough to allow tunneling transitions between the configurational states q_0 and q_1. In the case of the metastable defects, V_0 is of the order of 1 eV. Transitions from the ground state q_0 into the metastable state q_1 can then be stimulated by illumination. A decay of the metastable state becomes possible at elevated temperatures.

quence, the occupancy of the states q_0 and q_1 during the external excitation will differ from that in thermal equilibrium. After the excitation is turned off, all states q_1 with $V_0(q_1) \gg k_B T$ will be frozen into the corresponding metastable configuration. A relaxation into the equilibrium ground state q_0 is possible, e.g., by annealing of the material. Depending on the magnitude of the available external energy E_{ex}, in this second case the differences between a crystalline and an amorphous solid will be more of a quantitative nature, reflecting the different numbers of states with a given value of ΔE and V_0 realized in the system.

In recent years a popular material for the study of both aspects mentioned above, i.e., of two-level systems and externally induced metastable configurational changes, has been hydrogenated amorphous silicon, *a*-Si:H. Whereas the influence of TLS on the properties of this material (e.g., Refs. 2 and 3) is of interest mostly from a purely physical point of view, an understanding of the metastable changes observed in *a*-Si:H appears to be crucial for the optimization of properties related to its present and future commercial applications. It is therefore this second point that has attracted much attention and is also the subject of our investigation.

The observation of metastable changes in *a*-Si:H goes back to the work of Staebler and Wronski,[4] who found in 1977 that the dark conductivity and photoconductivity of glow-discharge-deposited amorphous silicon can be reduced significantly by prolonged illumination with intense light. The observed changes were found to be reversible by annealing of the *a*-Si:H samples at elevated temperatures ($\geq 150\,^{\circ}\mathrm{C}$), and were attributed to a reversible increase of the density of gap states acting as recombination centers for photoexcited carriers and leading to a shift of the dark Fermi level E_F toward midgap.[4] Since this first report, light-induced metastable changes in the properties of hydrogenated amorphous silicon are referred to by the name Staebler-Wronski effect (SWE) and have been studied quite intensively as reflected by a large number (> 100 at present) of related publications.

The majority of these subsequent investigations has been directed toward an understanding of the reversible changes in the density of localized gap states of *a*-Si:H and a documentation of resulting changes in the electronic, optical, and magnetic properties of this material. Direct evidence for the creation of states in the mobility gap of *a*-Si:H by prolonged illumination comes from a variety of experiments: reversible changes in the field effect,[5,6] the deep-level transient spectroscopy response,[7] defect luminescence,[8] subgap absorption,[9] and, more specific, from an increase of the Si dangling-bond signal in electron-spin resonance.[10,11] Apart from these direct measurements of the light-induced increase of the defect density in *a*-Si:H, an even larger number of studies has deduced a similar effect of illumination from the changes observed in almost any macroscopic property of amorphous silicon. Most commonly, the reversible changes in the transport properties of *a*-Si:H, measured with a variety of experimental techniques on different diode structures, are used to investigate the SWE.[12–21] Additional information comes from time-resolved or steady-state measurements of optical properties.[8,9,22–25]

It turns out to be very difficult to account for the large amount of experimental data mentioned so far in a consistent way. The conclusions of different authors agree qualitatively in that illumination with intense light leads to the creation of additional metastable states in the gap of amorphous silicon which influence its electronic and optical properties by decreasing the lifetime of excess carriers and shifting the position of the dark Fermi level in a reversible manner. The quantitative conclusions from the different experiments, however, do not agree at all. Discrepancies exist as to the absolute density of the metastable defects, their position in the mobility gap, and whether one or more types of defects can be created by illumination. Another important question that has remained unanswered until now is whether the SWE is mainly related to the bulk or to the surface properties of a given *a*-Si:H sample. At present, experimental evidence exists for either of the two extreme interpretations as well as for models considering reversible changes both in the bulk and the surface density of states.[13,18,26–31]

Given the small agreement between the different experimental results, it is not astonishing that our understanding of the microscopic mechanisms leading to the SWE is, at best, rudimentary. In addition to the group of experiments linking the SWE to reversible changes in the gap-state density of *a*-Si:H, a number of experiments performed on Schottky diodes, solar cells (*p-i-n* diodes), or on *n-i-n* and *p-i-p* structures have been very informative as far as the origin of the SWE is concerned.[13,32–36] It follows conclusively from these experiments that the recombination of excess carriers is responsible for the creation of metastable defects in undoped ("intrinsic") amorphous silicon, independent of whether the excess carriers are created by illumination or, for example, by double injection in a forward-biased *p-i-p* diode. (It should be mentioned, however, that recent results on *p-i-p* diodes suggest the possibility of reversible changes to a small degree by trapping of holes alone.[36])

Based on these experimental results, several microscopic processes have been proposed to explain the SWE. The first one involves the separation of weak Si—Si bonds into one or two Si dangling bonds and is, therefore, known as the "bond-breaking" model. This mechanism, together with a possible rearrangement of hydrogen atoms in *a*-Si:H, has been put forward by Elliott,[37] Staebler and Wronski,[13] Morigaki *et al.*,[22] Pankove and Berkeyheiser,[8] and, in more detail, by Dersch *et al.*[11] A different picture of the SWE involves reversible changes in the charge or hybridization state of already existing dangling bonds. This kind of mechanism has been proposed by Adler[38,39] and by Wautelet *et al.*[40] Finally, there has been some experimental evidence that the magnitude of the SWE increases with the concentration of impurities like oxygen, nitrogen, or carbon in *a*-Si:H.[41–44] This observation has led to a model according to which the SWE is not intrinsic to *a*-Si:H, but rather linked to the presence of impurities in special microscopic configurations.

In addition to the experimental results mentioned so far, there has been in recent years an increasing number of investigations dealing with reversible changes in the prop-

erties of doped and compensated amorphous silicon.[45–49] Among the interesting phenomena observed in doped material are an increase of the induced metastable states with increasing boron or phosphorus doping[48] and the occurrence of a "negative Staebler-Wronski effect" in compensated or lightly doped samples.[45,47] However, in this paper we will focus our attention on undoped *a*-Si:H, because we feel that doping introduces additional degrees of freedom for structural changes in *a*-Si:H which will not be available in undoped samples. Therefore, the conceptually safest approach towards the SWE seems to be an in-depth study of undoped material.

We have undertaken such a systematic study using electron-spin resonance (ESR) and photoconductivity (PC) as the experimental tools to monitor reversible changes in our samples both from a microscopic and macroscopic point of view. According to the different aspects of the SWE investigated here, the presentation and the discussion of our experimental results will be divided into five sections. In the first section we will briefly discuss the influence of the internal parameters—sample thickness and impurity concentration. The largest portion of this paper will be devoted to an investigation of the effect of the external parameters—illumination time, light intensity, photon energy, and illumination and annealing temperature, with special emphasis on the kinetics of the metastable defect creation and annealing in subsections B and C. In the last section we will attempt to reconcile our experimental results in a microscopic picture of the SWE.

II. EXPERIMENT

Undoped *a*-Si:H samples in the thickness range from 0.1 to 7 μm were deposited by rf glow discharge of pure SiH_4 either in a conventional, but baked system, or in an ultrahigh-vacuum (UHV) deposition system. For a detailed description of the latter system, see Ref. 50. The deposition parameters used were a flowrate of 100—150 sccm pure silane, a rf power of 2 W, and a substrate temperature of 230 °C. Generally, Corning 7059 substrates (0.5×1 cm^2) were used. The impurity content (carbon, oxygen, nitrogen, chlorine) of the samples was determined by secondary ion-mass spectroscopy (SIMS) profiling.

The electron-spin-resonance measurements were performed with a Varian E 201 *X*-band spectrometer in conjunction with an Air Products cryostat for temperature-dependent measurements in the range 10—500 K. The modulation amplitude and microwave power of the spectrometer were optimized for detection of the silicon dangling-bond signal ($g=2.0055$), resulting in a detection limit of 6×10^{11} dangling bonds at room temperature. This limit corresponds to a minimum detectable spin density of 10^{15} cm^{-3} in a typical sample (0.5 cm$\times$1 cm$\times$3 μm). To avoid errors introduced by varying the position of a sample in the microwave cavity for consecutive measurements, illumination and annealing were performed mostly inside the cavity itself without removing the sample. Depending on the kind of experiment, two sampling techniques were used. In cases where a measurement of the ESR signal was not disturbed by time-dependent variations of the number of dangling bonds, the complete spectral information was obtained by averaging three or more scans of the static magnetic field H across the dangling-bond resonance ($H=H_0$). This conventional ESR sampling mode is possible (and more accurate), for example, during illumination of a sample at temperatures below 100 °C. In this case the illumination can be interrupted and the number of dangling bonds will remain unchanged during the time necessary for an accurate measurement (15 min). This conventional method fails, however, at temperatures above 100 °C because annealing of the metastable dangling bonds leads to a noticeable decrease of the ESR signal during the time necessary for the recording of a complete ESR spectrum. Therefore, in this temperature regime, the following double-modulation technique was employed. The static magnetic field H is fixed at the resonant value H_0. Then 100-kHz modulation of this static field is used to allow the usual lock-in detection of the ESR signal. However, in addition a second pair of modulation coils is operated with a low frequency (typically 10 Hz) and a modulation amplitude equal to $\Delta H_{pp}/2$, where ΔH_{pp} is the peak-to-peak linewidth of the ESR signal to be detected. The output of the first high-frequency lock-in stage is analyzed by a second phase-sensitive detector locked to the second, low-frequency modulation. This mode allows fast, continuous, and accurate measurement of the amplitude of the conventional single-modulation ESR signal, provided that the line shape of this signal does not change significantly with time. Fortunately, this is fulfilled in the case of the SWE. The line shape of the stable dangling bonds is in first order the same as that of the metastable dangling bonds. Thus the line-shape information gained in a usual ESR experiment becomes redundant and can be traded in for a faster or more accurate intensity information. It should be mentioned, however, that small but significant differences between the line shapes of stable and metastable dangling bonds exist. These will be discussed in a later publication.

Measurements of the photoconductivity in our samples were performed by evaporating chromium co-planar bottom electrodes with a gap of 0.5 mm on the substrates prior to the glow-discharge deposition. Both, chopped illumination combined with lock-in detection and continuous illumination were used. The intensity dependence of the PC was measured using neutral-density filters. For direct comparison, the reversible change of the PC during illumination together with that of the dangling-bond density was measured simultaneously while a sample was illuminated inside the microwave cavity.

Several light sources were employed for illumination of the different samples. Reproducible transformation of samples with various thickness from the annealed state *A* to the light-soaked state *B* was obtained by prolonged illumination ($\geq$16 h) with unfiltered white light (350 mW/cm^2) from a tungsten lamp in a fixed configuration. Well-defined illumination conditions necessary for the investigation of the defect-creation kinetics were realized by the use of monochromatic light from a Kr^+ laser (647.1 nm, $h\nu=1.91$ eV, or, for more homogeneous illumination, 676.4 nm, $h\nu=1.83$ eV). For the investigation of the photon-energy dependence of the SWE, we made use

of monochromatized light from an arc lamp. In all cases the sample heating resulting from the illumination was determined and taken into account for the final analysis.

Finally, for the transformation of an illuminated sample from state B to state A, the sample was either annealed on a hot plate in air at 165 °C for 1 h, or inside the microwave cavity in N_2 at various temperatures for up to 4 h. It was ascertained by SIMS measurements that annealing of a high-purity sample for as much as 24 h in air at 190 °C did not lead to a significant increase of the oxygen or nitrogen content in the surface or bulk of the samples. Therefore, the annealing procedures employed do not alter the bulk composition of the sample.

III. RESULTS AND DISCUSSION

A. The influence of internal parameters: Sample thickness and impurity concentration

Although our study is mainly concerned with the influence of externally variable parameters on the metastable changes in a given sample, we will begin with a brief description of our results concerning the influence of the thickness and the impurity content of a sample. These experiments address the questions of whether the SWE is caused by impurities in a-Si:H and whether it is a surface or a bulk effect. A detailed discussion of these two aspects of the SWE in amorphous silicon has been or will be given elsewhere.[51,52]

For an investigation of the effect of varying sample thickness on the magnitude of the SWE, the total number of dangling bonds created in samples with thicknesses between 0.1 and 7 μm by prolonged illumination was determined by ESR measurements. The results are shown in Fig. 2(a) for samples deposited in two different systems: a baked conventional glow-discharge apparatus and an UHV system. Following the straight line with slope 1 in this double-logarithmic plot, the number of induced dangling bonds first increases proportional to the sample thickness d up to about $d=0.5$–0.6 μm for both sets of samples. Thicker samples, however, do not show a further increase of the observed ESR signal. Since the light soaking in the case of Fig. 2(a) was performed with white light in thicker samples. Therefore, the experiment was repeated with weakly absorbed monochromatic light ($h\nu=1.8$ eV). Surprisingly, the results are the same [Fig. 2(b)]. In addition, the complete light soaking of the thick-

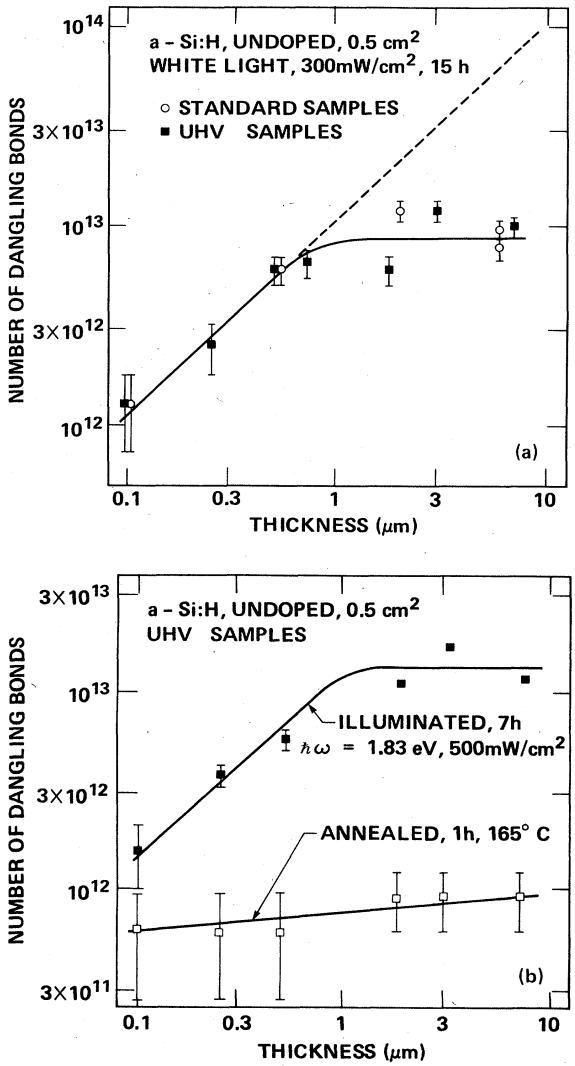

FIG. 2. Variation of the number of dangling bonds observed by ESR after prolonged illumination with sample thickness. (a) Illumination with white light for UHV samples (solid squares) and standard glow-discharge samples (open circles). (b) Illumination with homogeneously absorbed monochromatic light (1.83 eV) for UHV samples. The open squares show the number of dangling bonds in the annealed state.

(hν=1.8 eV). Surprisingly, the results are the same [Fig. 2(b)]. In addition, the complete light soaking of the thicker samples was checked by prolonged illumination from both sides. Our data lead to the conclusion that a two-phase model is necessary to describe the SWE in thick samples. According to this model, one or more regions with a combined thickness of approximately 0.5 μm exist, which are highly susceptible for light-induced metastable changes, whereas the rest of the sample is, by about an order of magnitude, more insensitive to the same kind of illumination. Similar results have been repeatedly reported for the thickness dependence of a variety of electronic properties both for the thermally equilibrated and the light-soaked states of a-Si:H.[30,53,54] Note as well that the thickness dependence of the ESR signal in the annealed state for the present high-quality films according to Fig. 2(b) can be separated into a surface contribution of about 10^{12} spins/cm^2 and a bulk spin density of 3×10^{15} cm^{-3}, in accordance with previous measurements.[55]

The present results suggest that there is both a surface and a bulk contribution to the SWE. Clearly, a purely surface-related origin has to be excluded, since a highly susceptible layer of about 0.5 μm thickness can hardly be referred to as a surface. On the other hand, it is clear that the bulk of the material is much less susceptible to the metastable changes. All this shows that in the context of the SWE (as well as in many other cases) amorphous silicon films show a considerable nonuniformity. There are

several possible causes for the observed inhomogeneity in the magnitude of the SWE. Nonuniform illumination conditions have already been excluded as discussed above. Thermal gradients caused by the illumination are negligible, as well, since due to the high thermal conductivity of *a*-Si no significant thermal gradients can be sustained, even in a 10-μm-thick sample. The next step, therefore, is to look for more structure-related inhomogeneities like profiles of hydrogen or impurity concentrations. Although it is known from SIMS or nuclear activation analysis that such profiles exist in *a*-Si:H, they are restricted to a total sample thickness of typically less than 0.1 μm,[50,56] and thus do not appear to be the cause for the inhomogeneous SWE. More promising candidates for an explanation of the measured thickness dependence are the existence of sample regions with considerable band bending near the free surface or the substrate/sample interface[27,56,57] and the high mechanical stresses reported for glow-discharge *a*-Si:H samples deposited on various substrates.[58–60] Band bending could affect the efficiency of metastable defect creation via changes in the recombination processes as discussed further below, and a possible negative influence of stress on the stability of bonds is conceptually easy to understand, even if detailed mechanisms are far from being positively identified. Both possibilities for an explanation of the observed thickness dependence are currently the subject of detailed investigations.

The second internal parameter that we have studied more closely is the concentration of the major impurities, oxygen and nitrogen, in the *a*-Si:H films. Again, the magnitude of the light-induced changes can be measured conveniently by comparing the intensity of the dangling-bond ESR signal in the annealed state, *A*, and after light soaking, state *B*, for samples with comparable thicknesses. In Fig. 3, the obtained spin densities are plotted as a function of the N and O concentration in the films. It can be seen that the SWE is independent of the impurity concentration below about a tenth of an atomic percent, with a typical increase of the defect density by about 1 order of magnitude from 10^{16} to 10^{17} cm^{-3} after prolonged illumination. This result shows quite conclusively that the SWE is intrinsic to *a*-Si:H, and not related to defect states created by incorporation of oxygen or nitrogen. Although not shown explicitly, similar conclusions are valid for a third major impurity, carbon. An influence of the incorporated impurities is only observed for higher concentrations of nitrogen or oxygen. In this range both the density of stable and metastable defects increases strongly with the impurity content. Previous studies reporting an increase of metastable changes with impurity concentration, actually, were performed always in this high-impurity-concentration region[41] and are therefore in accordance with the present results. The low-impurity-concentration regime has only recently become accessible by the use of UHV systems.[52] It follows from Fig. 3, however, that the large investments connected with an UHV deposition system will not be rewarded by a better stability of the *a*-Si:H films, once the critical impurity concentration of about 10^{19} cm^{-3} has been reached. The detailed mechanisms for the enhancement of the reversible changes in the high-impurity-concentration regime are not known at this point, but it is plausible that high contents of impurities will result in significant changes of the bonding structure in *a*-Si:H. This could lead to a greater susceptibility of the material for light-induced structural reactions. Such a "softening" of the Si network is also suggested by the observed increase of stable dangling bonds with increasing nitrogen or oxygen content above 10^{20} cm^{-3}.

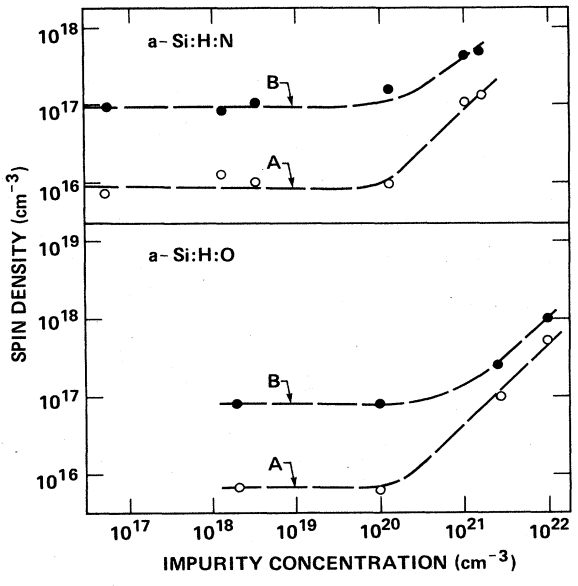

FIG. 3. Dependence of the ESR spin density in the annealed state (*A*) and the light-soaked state (*B*) on the concentration of nitrogen (upper part) and oxygen (lower part) present in *a*-Si:H.

B. Kinetics of metastable defect creation

The results of the preceding subsection indicate that the SWE is most likely intrinsic to hydrogenated amorphous silicon. The final goal in understanding the creation of metastable defects is, therefore, to identify one (or maybe more) microscopic process(es) possible in pure *a*-Si:H, i.e., processes not involving impurity atoms other than hydrogen, which are compatible with the various experimental results. Ultimately, any serious model for the SWE especially has to be able to explain the kinetics of the defect-creation process, i.e., the dependence of the number of created metastable defects on the external parameters—illumination time and illumination intensity. Surprisingly, there have only been very few investigations dealing with this kinetic behavior of the SWE in a quantitative way.[61–64] In this section, we will discuss in detail a kinetic model for the SWE recently proposed by us.[65,66] For the sake of clarity, we will first develop the kinetic theory, and then compare the predictions of this model for the metastable changes of the PC and ESR response with the experimental data. This will be followed by a discussion of our model in the context of other existing theoretical or experimental investigations.

1. Theory of kinetic behavior

In our model the defect creation in an a-Si:H sample under steady-state illumination occurs by nonradiative recombination between optically excited electrons (n) and holes (p). Therefore, it is imperative for an understanding of the effect to develop a sufficient description of the excess carrier distribution under these conditions. To obtain such a description in detail has been impossible up to date. Fortunately, the details of the carrier distribution turn out to be relatively unimportant for the kinetic modeling of the SWE if one restricts the validity of such a model to the high-temperature regime, $T > 200$ K. In this case the lifetime of excited carriers is sufficiently short ($\tau < 1$ ms), and the thermal energy $k_B T$ is comparable to the decay constant $E_0 \approx 50$ meV of the exponential band tails, so that thermal equilibrium between the band tails and extended states is readily achieved. It is then possible and useful for the following to define the integral concentrations n and p of excited electrons and holes by the two (coupled) equations

$$n = \int_{\mathrm{CB}} f_n(E,T,G,N_r,p)\rho(E)dE \ , \tag{1a}$$

$$p = \int_{\mathrm{VB}} f_p(E,T,G,N_r,n)\rho(E)dE \ . \tag{1b}$$

Here, CB denotes the energy region of the (shallow) conduction-band-tail states and above, VB the corresponding region of the valence band, $\rho(E)$ is the electronic density of states, and the occupation functions f_n and f_p for electrons and holes are functions of the energy E, the temperature T, the generation rate G, and the density N_r of recombination centers. In a-Si:H, a large number of experiments (e.g., Refs. 67–73) has shown conclusively that the main and possibly only type of recombination center is given by the three different charge states of the Si dangling bond,

$$N_r = N^+ + N^0 + N^- \ . \tag{2}$$

N^+ and N^- are the densities of the charged configurations of a dangling bond occupied by two holes (N^+) or two electrons (N^-) and are both diamagnetic. The usually observed ESR signal at $g = 2.0055$ ascribed to the dangling-bond defect originates from the neutral, singly occupied configuration N^0. Therefore, the number or density of dangling bonds or spins, N_s, always refers to this later concentration, $N_s = N^0$. Since it is known that the spin density N_s increases during illumination of a-Si:H, the SWE will influence the integral concentrations n and p via a variable density of recombination centers, $N_r = N_r(t_{\mathrm{ill}})$, where t_{ill} is the illumination time. The temperature T, the light intensity $I \propto G$ (generation rate), and the illumination time t_{ill} are the external parameters affecting the steady-state concentrations n and p. However, for now we will assume a constant temperature and concentrate on the kinetic parameters G and t_{ill}.

The relationship between n, p, and the population of the recombination centers N_r under steady-state illumination is governed by the detailed balance between the transitions shown in Fig. 4. Excess electrons and holes are created with a constant generation rate G. After the excitation, they thermalize rapidly into the shallow band-tail states and contribute to the PC via a multiple-trapping mechanism during a mean lifetime τ. This lifetime is limited by the recombination of the excess carriers. In the present picture a recombination is any event that removes an electron or hole from the integral populations n or p. This is possible by sequential deep trapping of a hole by a negatively charged (D^-) or neutral (D^0) dangling bond and of an electron by a neutral or positively charged (D^+) dangling bond. In addition, direct tail-to-tail transitions between excess electrons and holes are possible. The transition probabilities per final state for the various transitions are given by the (temperature-dependent) quantities A_p^-, A_p^0, A_n^0, A_n^+, and A_t as specified in Fig. 4. In principle, all of the recombinant transitions shown can occur radiatively, i.e., by emission of a photon (luminescence), or nonradiatively, that is, by a multiphonon process. The branching ratio between these two possible channels depends critically on the electron-phonon coupling of the initial states. At room temperature or above, the transitions are predominantly nonradiative.

Independent of the type of transitions prevailing, the dynamic situation in the model described by Fig. 4 will be completely characterized by the following set of rate equations:

$$dn/dt = G - n(A_n^0 N^0 + A_n^+ N^+ + A_t p) \ , \tag{3a}$$

$$dN^-/dt = nA_n^0 N^0 - pA_p^- N^- \ , \tag{3b}$$

$$dN^0/dt = n(A_n^+ N^+ - A_n^0 N^0) + p(A_p^- N^- - A_p^0 N^0) \ , \tag{3c}$$

$$dN^+/dt = pA_p^0 N^0 - nA_n^+ N^+ \ , \tag{3d}$$

$$dp/dt = G - p(A_p^0 N^0 + A_p^- N^- + A_t n) \ . \tag{3e}$$

This set of equations is simplified in so far as optically *excited* transitions from localized to localized and localized to extended states have been neglected in comparison to extended-extended absorption. Moreover, it will be shown in the Appendix that within certain limits the distinction between the different dangling-bond charge states D^+, D^0, and D^- can be omitted, leading to

$$dn/dt = G - n(A_n N_r + A_t p) \ , \tag{4a}$$

$$dN_r/dt = 0 \ , \tag{4b}$$

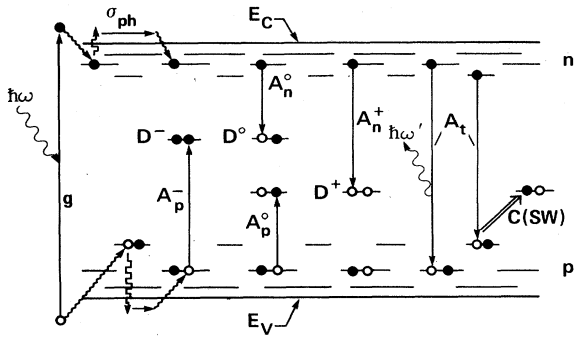

FIG. 4. Schematic diagram for the generation and recombination of excess electrons (n) and holes (p) in hydrogenated amorphous silicon. D^+, D^0, and D^- refer to the charge state of the dangling bonds prior to the electronic transition. See text for details.

$$dp/dt = G - p(A_p N_r + A_t n) , \tag{4c}$$

where

$$A_n N_r \equiv A_n^0 N^0 + A_n^+ N^+$$

and

$$A_p N_r \equiv A_p^0 N^0 + A_p^- N^-$$

are effective transition rates for excess electrons and holes being trapped by dangling bonds of all possible charge states. Note, however, that the simplification leading to (4) is only possible if the ratios $n^+ = N^+/N_r$, $n^0 = N^0/N_r$, and $n^- = N^-/N_r$ do not depend on the external parameters G and $t_{\rm ill}$, as discussed in the Appendix. Moreover, for Eq. (4b) to be a valid approximation, one has to make sure that the increase $dN_r/dt_{\rm ill}$ of the dangling-bond density resulting from the SWE occurs on a much longer time scale than the equilibration between the different populations in Fig. 4, as described by the rate equations above. This is the main reason why the following kinetic model is only valid in the high-temperature regime ($T > 200$ K), where the equilibration between the different occupancies will not be disturbed by the slowly increasing number of dangling bonds. In this case, a quasi-steady-state approach to the rate equations (4) is possible: $dn/dt = dp/dt = 0$. Thus, one obtains the integral populations n and p as

$$n = G/(A_n N_r + A_t p) , \tag{5a}$$

$$p = G/(A_p N_r + A_t n) . \tag{5b}$$

This pair of coupled equations can be solved by substitution and leads to the following expressions for n and p:

$$n = G/\{(A_n N_r/2) + [(A_n N_r/2)^2 + A_t A_n G/A_p]^{1/2}\} , \tag{6a}$$

$$p = G/\{(A_p N_r/2) + [(A_p N_r/2)^2 + A_t A_p G/A_n]^{1/2}\} . \tag{6b}$$

Neglecting possible small variations of A_p and A_n as described in the Appendix, these equations are generally valid and comprise both the limiting cases of purely bimolecular recombination at high intensities with

$$n = (A_p/A_t A_n)^{1/2} G^{1/2}, \quad p = (A_n/A_t A_p)^{1/2} G^{1/2} , \tag{7}$$

and that of purely monomolecular recombination at low intensities and/or high densities N_r of recombination centers:

$$n = G/(A_n N_r), \quad p = G/(A_p N_r) . \tag{8}$$

According to Eqs. (6a) and (6b), the transition between these two extremes is characterized by

$$(A_n N_r/2)^2 \approx A_t A_n G/A_p$$

and

$$(A_p N_r/2)^2 \approx A_t A_p G/A_n ,$$

and occurs around

$$G/N_r^2 \approx A_n A_p/4A_t . \tag{9}$$

We are now in the position to derive the kinetic behavior of the metastable defect creation. As indicated in Fig. 4, our model is based on the assumption that new metastable dangling bonds are created by the fraction of nonradiative, direct tail-to-tail recombination transitions. This is suggested by the experimentally observed dominant role of recombination in the defect-creation mechanism and by the fact that nonradiative transitions can provide, in the form of local phonons, the energy necessary to surmount the potential barrier of about 1 eV separating the stable ground state from the metastable defect state (cf. Fig. 1). At this point we will not try to describe a detailed microscopic process for the metastable defect creation. This will be the subject of subsection E. We rather continue with the development of the kinetic behavior resulting from such a model. Therefore, if we accept that new dangling bonds are created by (nonradiative) tail-to-tail transitions, we are led to the following equation for the change of the dangling-bond density N_r with illumination time $t_{\rm ill}$:

$$dN_r/dt_{\rm ill} = c_{\rm SW} A_t n p . \tag{10}$$

Here, $A_t np$ is the number of tail-to-tail transitions per unit time and volume, and $c_{\rm SW}$ is a constant describing the average efficiency of these transitions for the creation of new dangling bonds.

Using the expressions for n and p given in Eqs. (6a) and (6b), we obtain the following differential equation for $N_r(t_{\rm ill})$:

$$dN_r/dt_{\rm ill} = (c_{\rm SW} A_t A_n G^2/A_p)\{(A_n N_r)^2/2 + A_n N_r[(A_t A_n G/A_p) + (A_n N_r/2)^2]^{1/2} + (A_t A_n G/A_p)\}^{-1} . \tag{11}$$

This equation can be integrated easily by separation of the variables, yielding the final relation for the illumination time and intensity dependence of the dangling-bond density:

$$[N_r^3(t_{\rm ill}) - N_r^3(0)] + (2/A_n)^3\{[A_n^2 N_r^2(t_{\rm ill})/4 + (G A_t A_n/A_p)]^{3/2} - [A_n^2 N_r^2(0)/4 + (G A_t A_n/A_p)]^{3/2}\}$$
$$+ 6G A_t [N_r(t_{\rm ill}) - N_r(0)]/(A_n A_p) = 6 c_{\rm SW} A_t G^2 t_{\rm ill}/(A_n A_p) . \tag{12}$$

Equation (12) is exact, except for the introduction of the effective transition probabilities A_n and A_p as discussed in the Appendix. However, although an exact solution of the present problem is possible, this somewhat obscures the physical processes behind the characteristic kinetic behavior exhibited by the SWE because of the complex analytical expressions obtained. We will, therefore, discuss briefly the more transparent case of low illumination intensities, which, as shown in the Appendix, is a good approximation for the range of external parame-

ters used in this study. In this case, Eqs. (6a) and (6b) are approximated by Eq. (8), i.e., by a purely monomolecular behavior of the integral free-carrier densities n and p. If we insert Eq. (8) into Eq. (10), we obtain a simplified version of Eq. (11):

$$dN_r/dt_{\rm ill}=c_{\rm SW}(A_t/A_nA_p)(G/N_r)^2 \ . \tag{11'}$$

Equation (11') reveals an important characteristic of the SWE, which is somewhat buried in the exact equation (11). The rate of creation of new dangling bonds, $dN_r/dt_{\rm ill}$, decreases with the square of the density of already existing dangling bonds. The physical reason for this decrease is that the tail-to-tail transitions leading to the creation of metastable dangling bonds are effectively shunted by the recombination events via the main recombination centers, the existing stable or metastable dangling bonds. In this sense, the SWE is self-limiting, since the creation of new dangling bonds is inhibited by the already existing dangling bonds. This self-limiting behavior is the main reason why the metastable changes connected with the SWE are not simply proportional to the exposure $It_{\rm ill}$ of a given sample. This becomes evident when (11') is integrated, yielding

$$N_r^3(t_{\rm ill})-N_r^3(0)=3c_{\rm SW}(A_t/A_nA_p)G^2t_{\rm ill} \ . \tag{12'}$$

For sufficiently long illumination times $t_{\rm ill}$, when $N_r(t_{\rm ill})>2N_r(0)$, $N_r^3(0)$ can be neglected compared to $N_r^3(t_{\rm ill})$, and one can simplify

$$N_r(t_{\rm ill})=[3c_{\rm SW}(A_t/A_nA_p)]^{1/3}G^{2/3}t_{\rm ill}^{1/3} \ . \tag{13}$$

Equation (13) shows that the increase in the density of metastable dangling bonds is expected to be sublinear both in illumination intensity ($G^{2/3}$) and illumination time ($t_{\rm ill}^{1/3}$). The same relation is also obtained easily as the limit of Eq. (12) for long illumination times.

A second interesting case is the initial increase of N_r for weak exposure, i.e., the case of short illumination times $t_{\rm ill}$ and low light intensities $I\propto G$. As long as $G^2t_{\rm ill}$ is sufficiently small, it is clear from Eq. (12) that $N_r(t_{\rm ill})\approx N_r(0)$. In this case, (12) can be approximated by the following linear relationship:

$$[N_r(t_{\rm ill})-N_r(0)]\{N_r^2(0)+N_r(0)[N_r^2(0)+4GA_t/(A_nA_p)]^{1/2}+2GA_t/(A_nA_p)\}=2c_{\rm SW}A_tG^2t_{\rm ill}/(A_nA_p) \ . \tag{14}$$

Again, for low generation rates G one can simplify, thus obtaining

$$[N_r(t_{\rm ill})-N_r(0)]=c_{\rm SW}A_t[G/N_r(0)]^2t_{\rm ill}/(A_nA_p) \ , \tag{14'}$$

which also follows directly from Eq. (11') by replacing the derivative $dN_r/dt_{\rm ill}$ with its difference quotient, $\Delta N_r/\Delta t_{\rm ill}$. We note for the following discussion that in this regime the density of dangling-bond defects increases linearly in illumination time with a slope proportional to the efficiency constant $c_{\rm SW}$.

2. *Kinetics of metastable changes of the photoconductivity*

In this subsection we will use our theory for the metastable defect creation as developed in subsection B 1 to describe the reversible changes of the steady-state photoconductivity during illumination. A general expression for the PC, $\sigma_{\rm ph}$, can be obtained similar to the definition of the integral densities n and p in Eqs. (1a) and (1b):

$$\sigma_{\rm ph}=e\left[\int_{\rm CB}\mu_n(E)f_n\rho(E)dE+\int_{\rm VB}\mu_p(E)f_p\rho(E)dE\right] . \tag{15}$$

Here, $\mu_{n\ (p)}(E)$ are the effective mobilities of electrons (holes) with energy E. Equation (15) can also be written in the form

$$\sigma_{\rm ph}=e(\mu_n n+\mu_p p) \ , \tag{15'}$$

where μ_n and μ_p are the average (drift) mobilities for electrons and holes,

$$\mu_n=(1/n)\int_{\rm CB}\mu_n(E)f_n(E,T,G,N_r,p)\rho(E)dE \tag{16}$$

(analogous for μ_p). In the case of amorphous silicon, it is possible to assume relatively sharp mobility edges E_C and E_V for electrons and holes with $\mu_n(E)=\mu_p(E)=0$ for $E_V\le E\le E_C$, and $\mu_n(E)=\mu_{n,0},\mu_p(E)=\mu_{p,0}$ otherwise. Equation (15) then reduces to

$$\sigma_{\rm ph}=e(\mu_{n,0}n_0+\mu_{p,0}p_0) \ . \tag{17}$$

n_0 and p_0 are the densities of carriers in extended states. In this approximation, the dependence of the PC on the generation rate G and the density N_r of recombination centers is only given by the dependence of n_0 and p_0 on these external parameters, since to first order the extended-state mobilities $\mu_{n,0}$ and $\mu_{p,0}$ can be regarded as constant. In addition, because we have restricted our analysis to the high-temperature regime, the densities n_0 and p_0 of carriers in extended states will be simply proportional to the total densities n and p of optically excited electrons and holes. This allows us to express the PC as

$$\sigma_{\rm ph}=e(\mu_{n,0}\beta_n n+\mu_{p,0}\beta_p p) \ , \tag{18}$$

where $\beta_n=n_0/n$ and $\beta_p=p_0/p$. The metastable changes of n and p during prolonged illumination have been derived in the preceding section and are given by Eqs. (6a) and (6b). Equation (18), therefore, allows us to relate the changes in the PC to the metastable changes of the dangling-bond density N_r as given implicitly by Eq. (12). The resulting expressions can easily be evaluated numerically, but are somewhat complicated to discuss. We will, therefore, restrict our discussion of the PC to the case of low illumination intensities and/or high dangling-bond densities. Then n and p in Eq. (18) can be approximated by the monomolecular limits given in (8), leading to

$$\sigma_{\rm ph}=B(G/N_r) \ , \tag{19}$$

where

$$B=e(\mu_{n,0}\beta_n/A_n+\mu_{p,0}\beta_p/A_p)$$

is a constant independent of G. Combining Eq. (19) with

Eqs. (12′) and (14′) we thus obtain the asymptotic variation of the PC with illumination time and intensity given by

$$[\sigma_{ph}(t_{ill})]^{-3}-[\sigma_{ph}(0)]^{-3}=3(c_{SW}A_t/A_nA_pB^3)(t_{ill}/G) \tag{20}$$

in the long-time limit, and by

$$[1/\sigma_{ph}(0)]\{[1/\sigma_{ph}(t_{ill})]-[1/\sigma_{ph}(0)]\} = c_{SW}t_{ill}A_t/[A_nA_pB^2N_r(0)] \tag{21}$$

for short illumination times and/or small generation rates. Note that in both equations, (20) and (21), the expressions on the left-hand side are proportional to the product $c_{SW}t_{ill}A_t$.

3. *Comparison between kinetic theory and experiment*

In this section, we will use the experimentally observed metastable changes of the ESR spin density and of the steady-state PC to test the validity of our theoretical approach described above. The raw data for the number of light-induced, metastable dangling bonds, N_{ind}, in a sample with a volume of 1.5×10^{-4} cm^3, are shown in Fig. 5 as a function of illumination time for various intensities of the monochromatic illumination. All measurements were performed on the same sample. The number $N_s(0)$ of stable dangling bonds at $t_{ill}=0$ (after annealing) is indicated by the dotted line. Annealing restores this value of $N_s(0)$ within the experimental accuracy. The different curves in Fig. 5 show a common behavior in that the number of induced spins first increases rapidly with illumination time. For longer times, however, N_{ind} seems to reach a saturated value, which, in turn, depends on the illumination intensity I.

In the context of our kinetic model, the dependence of the dangling-bond density on t_{ill} and I is given by Eq. (12). We first note that according to the Appendix the density (or number) of metastable and stable paramagnetic dangling bonds, $N_s=N^0$, is expected to be a constant fraction n^0 of the total density (or number) of dangling bonds, N_r, appearing in Eq. (12) [cf. Eq. (A11)]. Secondly, for a comparison with Eq. (12), we should not plot the number of *induced* dangling bonds, N_{ind}, as in Fig. 5, but the *total* number of dangling-bond related spins, $N_s=N_{ind}+N_s(0)$, as a function of the illumination time. This has been done in Fig. 6, using a double-logarithmic plot. Figure 6 nicely shows the long-time behavior of the total spin density. When $N_s(t_{ill})>2N_s(0)$, as indicated by the dashed line, all curves exhibit a $t^{1/3}$ dependence on illumination time within the experimental accuracy. Moreover, the inset in Fig. 6 shows that the intensity dependence of N_s for a fixed length of illumination is close to $I^{0.6}$ in this long-time limit. This dependence of $N_s\propto t_{ill}^{1/3}I^{0.6}$ compares very favorably with the kinetic model, which according to Eq. (13) predicts a dependence as $t_{ill}^{1/3}I^{2/3}$. For a more detailed comparison over the whole time range, a numerical analysis of Eq. (12) is necessary. The results of such a comparison are shown in Fig. 7–9. We would like to stress the point that for a fit between the experimental results and theoretical predictions only one free parameter is available, namely the product $c_{SW}A_t$ of the dangling-bond creation efficiency and the tail-to-tail transition probability. All other quantities in Eq. (12) are determined from other experiments and, therefore, are not free fitting parameters. $c_{SW}A_t$ can be evaluated most easily by fitting the theoretical curves to the actual data points for a sufficiently high illumination intensity in the $t^{1/3}$ regime. Figure 7 demonstrates this for an illumination intensity of 400 mW/cm^2, assuming a value of $c_{SW}=5\times10^{-5}$. Then, $A_t=3\times10^{-11}$ cm^3 s^{-1} is obtained from the fitting procedure, consistent with the experimentally observed transition from a monomolecular to a bimolecular recombination according to Eq. (9). This gives us $c_{SW}A_t=1.5\times10^{-15}$ cm^3 s^{-1}, and we will use this value throughout the rest of this paper. Note that in Fig. 7 the spin-density values at short times deviate somewhat from the theoretical curve that fits the

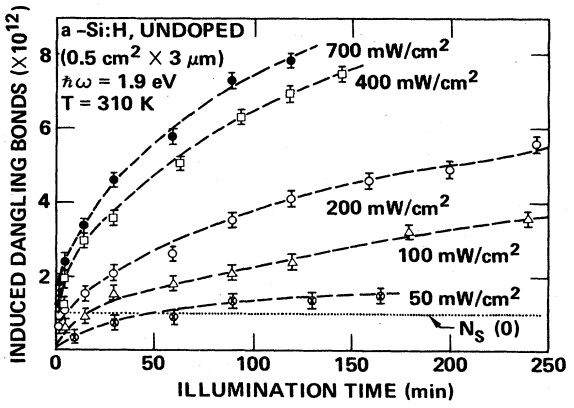

FIG. 5. Increase of the number of light-induced metastable dangling bonds (determined by ESR) as a function of illumination time for various light intensities. Experiments were done on the same sample at room temperature using monochromatic laser light (1.9 eV). The dotted line $N_s(0)$ indicates the level of stable dangling bonds measured after annealing of the sample.

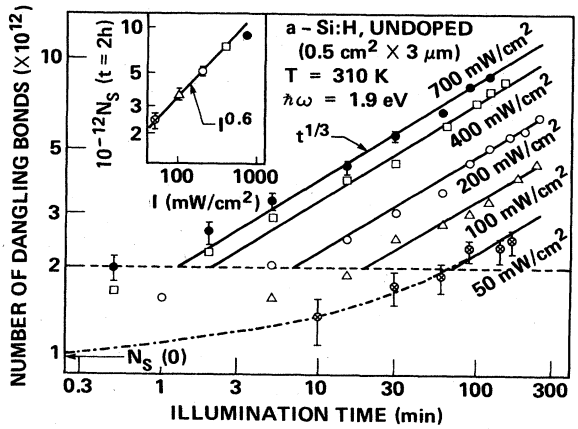

FIG. 6. Double-logarithmic plot of the data in Fig. 5. Note that instead of the number of *induced* dangling bonds the *total* number of dangling bonds has been plotted here. For $N_s>2N_s(0)$ (dashed line) all curves follow within the experimental error a $t^{1/3}$ time dependence. The inset shows that the dependence on light intensity in this regime is given by $I^{0.6}$.

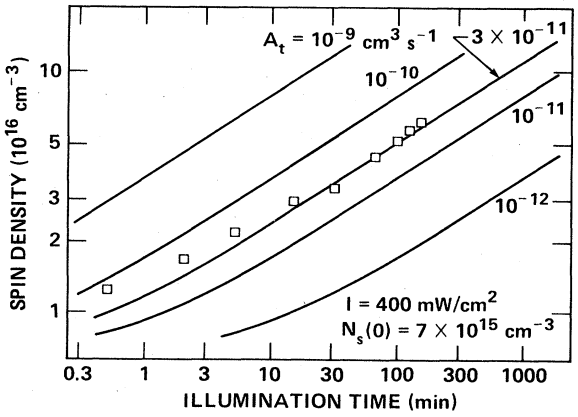

FIG. 7. Theoretical variation of the total spin density with illumination time for different tail-to-tail transition probabilities A_t. Here a creation efficiency of $c_{SW}=5\times10^{-5}$ has been assumed. The open squares are the experimental points for an illumination intensity of 400 mW/cm^2 taken from Fig. 6. The best fit to the long-time behavior is obtained for $A_t=3\times10^{-11}$ cm^{3}s^{-1}.

same set of data at long illumination times. This disagreement is partly due to the relatively larger error bars for the low-spin-density points. On the other hand, the short-time regime is strongly dependent on the starting dangling-bond density $N_s(0)$. This can be seen in Fig. 8, where theoretical curves are shown for $c_{SW}A_t$ as deduced above, however, allowing some variations in $N_s(0)$. A nearly perfect fit is obtained for $N_s(0)\approx1\times10^{16}$ cm^{-3}, which, indeed, is closer to the experimentally obtained value of $N_s=(9\pm3)\times10^{15}$ cm^{-3} than the density of 7×10^{15} cm^{-3} used in Fig. 7. For a single illumination intensity, therefore, the agreement between Eq. (12) and the experimental data is excellent. The same is true if we extend our comparison over a wide range of different illumination intensities, although now *no* free parameters are available. The comparison between the complete set of experimental results (of Fig. 6) and the kinetic model is shown in Fig. 9. For intensities up to 400 mW/cm^2, any deviation from the theoretical predictions would be smaller than the experimental uncertainty. Significant differences are only present for the highest intensity, $I=700$ mW/cm^2. The most likely reason for this disagreement is that sample heating due to the illumination is no longer negligible here (see the discussion of the temperature dependence below). Nevertheless, the conclusion from Fig. 9 is that the proposed kinetic model of the SWE can quantitatively explain our ESR results over 1 order of magnitude in illumination intensity and nearly 3 orders of magnitude in illumination time.

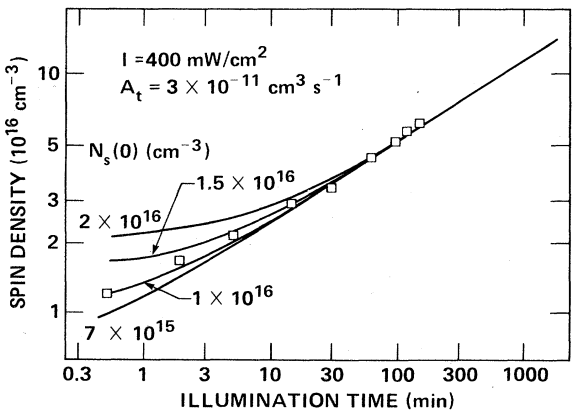

FIG. 8. Dependence of the short-time spin-density increase on the initial spin density $N_s(0)$. ($c_{SW}A_t=1.5\times10^{-15}$ cm^{3}s^{-1}.)

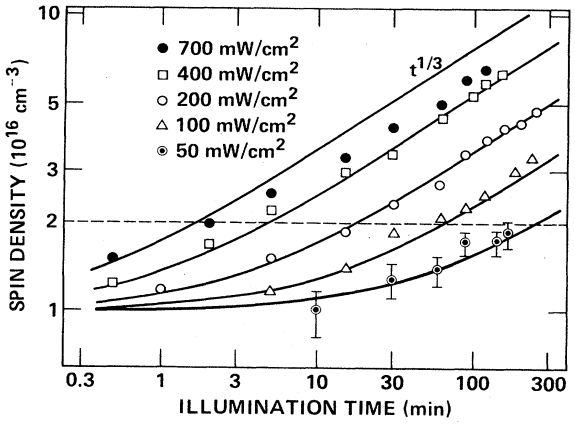

FIG. 9. Comparison between the theoretically predicted kinetic behavior of the spin density (solid lines) and the experimental data from Fig. 6. [$N_s(0)=1\times10^{16}$ cm^{-3}, $c_{SW}A_t=1.5\times10^{-15}$ cm^{3}s^{-1}.]

The applicability of the kinetic model is not limited to an explanation of the ESR data alone. In the following we will show that the kinetic behavior of the PC, too, can be explained in the framework of the theoretical description developed in subsection B 2, above. The decrease of the photoconductivity with illumination time for three different light intensities is summarized in Fig. 10. The observed variation is similar to the kinetics of the ESR spin density in Fig. 5 in that the metastable changes are relatively large for short illumination and seem to saturate

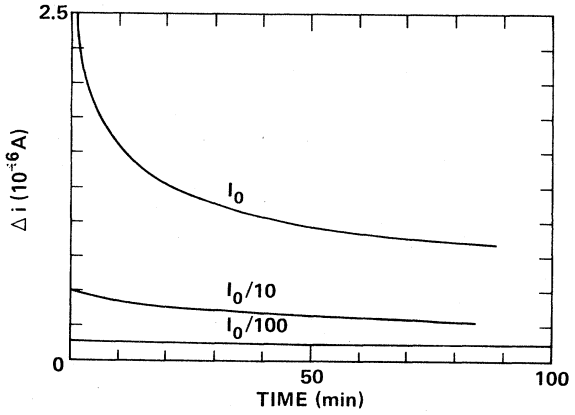

FIG. 10. Time dependence of the photocurrent Δi in undoped a-Si:H for three different illumination intensities (monochromatic illumination, $h\nu=1.9$ eV, $I_0=170$ mW/cm^2).

at longer times. Moreover, the absolute level of the PC as well as the magnitude of the reversible changes both decrease with decreasing illumination intensity. The decrease in the PC occurs parallel to the increase of the dangling-bond density, as predicted by Eq. (19). Before analyzing this behavior in more detail, it is useful to ascertain the validity of this central equation, i.e., the proportionality of the PC to the illumination intensity I and to the inverse dangling-bond density $1/N_s$. Figure 11 shows that the PC, indeed, is nearly proportional to the incident light intensity over 6 orders of magnitude. The observed dependences are $\sigma_{ph} \propto I^{0.92}$ in the annealed state, and $\sigma_{ph} \propto I^{1.04}$ after prolonged illumination with the strongest intensity ($I_0 = 200$ mW/cm^2) employed in the measurements shown.

These results are somewhat in disagreement with a large number of similar investigations reporting intensity dependences of the PC as I^γ, with γ varying typically between 0.5 and 1.[13,74–77] The reasons for this largely varying intensity dependence are still not fully understood. We would like to point out, however, that special care has to be taken to avoid the introduction of experimental artifacts into the intensity dependence of the PC. A common source of error is the use of light sources leading to nonuniform illumination of the sample, especially in combination with gap contacts on the illuminated top surface. In this study we have, therefore, used monochromatic light with sufficiently long wavelength, and bottom contacts to reduce contact-related irreversible changes during the thermal anneals of our samples. A second source of error is the influence of surface band bending on the obtained intensity dependence.[77] In particular, thin films ($d < 0.5$ μm) are dominated by surface effects and exhibit values of γ significantly smaller than 1. Therefore, we used only thick films ($d = 3$ μm) for the investigation of the kinetic behavior. A third problem in measuring the exponent γ for a low-defect-concentration a-Si:H sample in the annealed state is the change of the dangling-bond density N_s during the PC measurement itself at higher illumination intensities. This complication cannot be avoided completely, but can be minimized by starting a measurement at the highest intensities and limiting the illumination to a period just long enough to reach steady state. Otherwise, γ will appear smaller than it actually is, because the induced dangling bonds reduce the photoconductivity for all subsequent points. For example, the intensity dependence in the annealed state could show a transition to a $I^{0.5}$ behavior, if one were to measure upwards in intensity.

The dependence $\sigma_{ph} \propto 1/N_s$ in Eq. (19) has been verified by using the same sample, provided with bottom chromium gap electrodes, for the PC and ESR measurements. The increase of the dangling-bond density and the resulting decrease of the photocurrent were monitored simultaneously while the sample was illuminated inside the microwave cavity with monochromatic light of intensity $I_0 = 300$ mW/cm^2. The decay of the PC at this high intensity was recorded continuously and results in the curve labeled "dc" in Fig. 12. At certain intervals, the illumination was interrupted for typically 10 min to allow an accurate measurement of the dangling-bond density N_s and, at the same time, a determination of the PC at lower intensities, $I_0/100 = 3$ mW/cm^2, using lock-in detection. These later results led to curve "ac" in Fig. 12. It can been seen from this curve that the low-intensity PC actually follows the monomolecular behavior of Eq. (19) within experimental accuracy. The high-intensity PC exhibits a slightly weaker N_s dependence, $\sigma_{ph}(\text{dc}) \propto N_s^{-0.85}$. This dependence of $\sigma_{ph} \propto N_s^{-1}$ has also been observed experimentally by other investigators, at least for high dangling-bond densities ($> 10^{17}$ cm^{-3}) (e.g., Ref. 63). However, for lower spin densities, σ_{ph} has been found to be nearly independent of N_s, in contrast to the present results which show the proportionality between σ_{ph} and N_s^{-1} down to a density of about 10^{16} cm^{-3} (cf. Fig. 12). Again, there are several possible reasons for this apparent

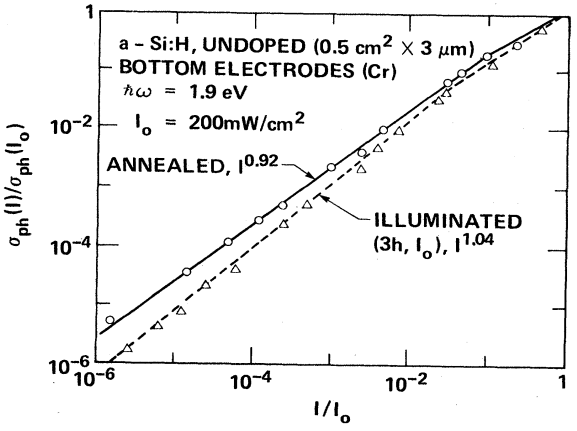

FIG. 11. Intensity dependence of the steady-state photoconductivity in the light-soaked state ($I^{1.04}$) and the annealed state ($I^{0.92}$).

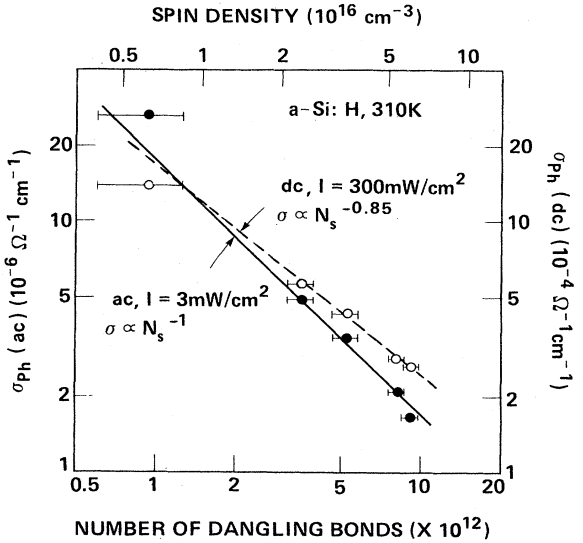

FIG. 12. Variation for the photoconductivity and the number of dangling bonds measured simultaneously during illumination of a sample inside the microwave cavity. ac: photoconductivity at low light intensities obtained with chopped light and lock-in amplifier. dc: high-intensity photoconductivity for continuous illumination.

discrepancy. We have already mentioned above experimental artifacts that can explain differences in the values obtained for σ_{ph} under supposedly identical conditions. In addition, the dependence of σ_{ph} is subject to errors introduced via the determination of the dangling-bond density by ESR. Here a problem is the large density of surface spins in a-Si:H, which typically lies between 1×10^{12} and 5×10^{12} cm^{-2} [see, for example, Fig. 2(b)]. In thin samples, the surface spins can dominate the ESR spectra up to bulk densities of 10^{17} cm^{-3}. So, in order to obtain the correct dependence of σ_{ph} on N_s one has to use sufficiently thick samples.

We conclude from Figs. 11 and 12 that the monomolecular approximation, Eq. (19), is sufficient to describe the spin density and intensity dependence of the PC in the range of illumination intensities used for this study. Therefore, Eqs. (20) and (21) should describe the long- and short-time kinetic behavior of the PC accurately. To test this, in Fig. 13 the raw data of Fig. 10 have been plotted according to Eq. (20). For the sake of comparability, the three curves in Fig. 13 have been scaled by the factor $1/G$ in Eq. (20). As expected, straight lines are obtained for the higher intensities $I_0=170$ mW/cm^2 and $I_0/10=17$ mW/cm^2. For the curve obtained at the lowest intensity, $I_0/100=1.7$ mW/cm^2, however, Eq. (20) is no longer valid, since it is based on the long-time limit, Eq. (13), of the spin-density variation. Indeed, a straight line is obtained for the low-intensity data if we use a linear plot according to Eq. (21), which describes more accurately the case of small total exposure. We will come back to this limit when discussing the photon-energy dependence of the metastable changes in subsection D. Note also that the intensity dependence of the slopes for the straight lines in Fig. 13 is close to the $1/G$ dependence as predicted by Eq. (19). This is shown in the inset of Fig. 13.

As mentioned above, we can obtain an exact description of the kinetic behavior of the PC by combining Eq. (18) with Eqs. (6a), (6b), and (12). However, this leads to implicit relations between σ_{ph}, G, and t_{ill} which no longer can be handled analytically. To conclude this comparison between experiment and kinetic theory, we therefore give

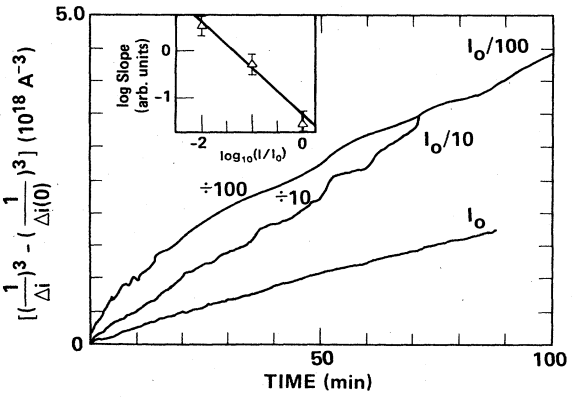

FIG. 13. Photoconductivity data of Fig. 10 plotted according to Eq. (20). For better comparison the curves have been scaled by $1/I$. The slopes of the unscaled curves are shown in the inset as a function of illumination intensity.

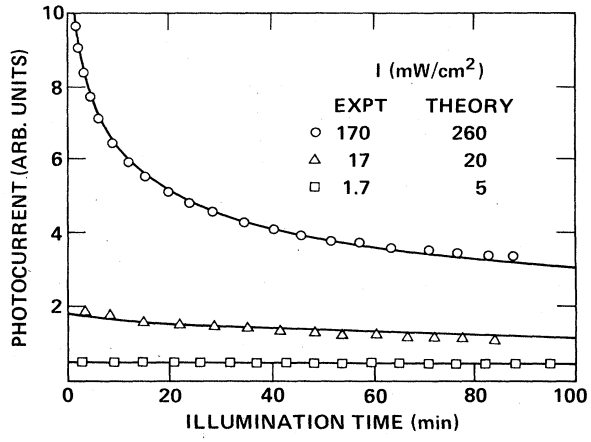

FIG. 14. Comparison of the experimental decay of the photoconductivity upon prolonged illumination (data points) with the theoretically predicted behavior (solid lines) for three illumination intensities.

in Fig. 14 the results of a numerical fit of the PC raw data in Fig. 10 to the general case of our theory. For this fit we have used the value of $c_{SW}A_t=1.5\times10^{-15}$ cm^{3}s^{-1} obtained from the ESR data. Therefore, *no* adjustable parameters are available for the fit in Fig. 14. As shown, small variations of the incident light intensities have to be allowed for a quantitative agreement. Note, however, that these differences mainly affect the absolute level of the PC, and not the relative time-dependent changes for a given intensity.

We can, therefore, summarize by saying that the present model provides a consistent, quantitative description of the metastable changes of both the photoconductivity and the dangling-bond density in undoped a-Si:H. In the next subsection, we will discuss this model in the context of other experimental and theoretical investigations.

4. *Comparison with existing experimental and theoretical investigations*

Although a detailed understanding of the defect-creation kinetics is an important aspect of the SWE, surprisingly few investigations have tried to deal with this problem in a quantitative way. Dersch reports an increase of the *induced* spin density, $N_{ind}=N_s(t)-N_s(0)$, proportional to $I^{0.75}$ and $t_{ill}^{0.39}$ upon illumination with white light for two samples with thicknesses around 1 μm.[63] These data can easily be reconciled with the present model by considering $N_s(t)=N_{ind}+N_s(0)$ rather than N_{ind} alone, as suggested by the common ability of both stable and metastable dangling bonds to act as recombination centers. A second set of data for the dependence of $N_s(t)$ on illumination time at different intensities similar to the results in Fig. 6 has recently been obtained by Lee *et al.*[64] These authors claim the observation of two time regimes: a $t^{1/3}$ behavior at high intensities and long illumination times, and a somewhat smaller time dependence for weak exposure. Again the data can be explained in the context of our kinetic model. The $t^{1/3}$ regime is in agreement

with Eq. (13), and the weaker time dependence for low illumination intensities, as long as $N_s(t) < 2N_s(0)$, also is evident from Fig. 9.

As far as the PC is concerned, the only quantitative approach toward a description of the kinetics of the metastable changes is given by Nitta *et al.*,[61] who use a superposition of a slow and a fast exponential decay component to quantify the PC decay. A fit is easily obtained because of the large number (four) of adjustable parameters. However, no physical justification for such a double-exponential decay of the PC was given. Moreover, the same experimental data can be fitted without difficulties to Eq. (19) in the present model. An interesting point mentioned by Nitta *et al.* is the degree of reversibility of the metastable defect creation. In the course of our ESR experiments, some samples were subjected to more than ten Staebler-Wronski cycles without showing any signs of irreversibility. On the other hand, Nitta reports irreversible changes of the conductivity already after one cycle. We believe, however, that these irreversible effects are caused by aging of the electrical contacts during the thermal anneal rather than by an incomplete anneal of created dangling bonds, since the latter ought to be observable in contactless experimental techniques such as ESR, luminescence, or optical absorption.

Finally, we would like to discuss how the kinetic model presented above fits into the two major microscopic theories proposed for the SWE, i.e., the bond-breaking model and the model involving negative-U dangling-bond sites. The specific kinetic behavior of the defect creation as discussed so far results from Eq. (10), which links the rate of creation, dN_r/dt, to the density N_r of existing dangling bonds via the product np of photoexcited carriers. As explained above, this relationship follows naturally from a bond-breaking model which assumes that new dangling bonds are created by tail-to-tail transitions occurring with a rate proportional to np. In the negative-U model, on the other hand, the total density N_r of dangling-bond sites is supposed to be constant, and only the hybridization and the charge state (D^+, D^0, D^-) are changed as a consequence of excess carrier capture. It is worthwhile to examine the kinetic behavior in the context of such a model, since this will allow us to determine the compatibility of the negative-U model with the experimental data.

The negative-U model as proposed by Adler[38] assumes that the majority of the dangling bonds can lower their total energy by the reaction $2D^0 \leftrightarrows D^+ + D^-$. The energy gain comes from the additional attractive Coulomb interaction between the charged dangling bonds if their spatial separation is sufficiently small, and from possible charge-induced local lattice relaxation: This leads to an overall negative effective correlation energy U. Isolated dangling bonds still can have a positive correlation energy, and can, therefore, be regarded as the origin of the usual ESR signal, since they are stable in the neutral, paramagnetic state. The SWE, then, arises from the capture of excess electrons or holes by the negative-U complexes, according to the reactions $D^+ + D^- + n \leftrightarrows D^0 + D^-$ and $D^+ + D^- + p \leftrightarrows D^+ + D^0$, which lead to the observed increase of the neutral dangling bonds, D^0. The creation of dangling-bond states with positive correlation energy, N_r, out of the reservoir of dangling bonds with negative correlation energy, $T = T^+ + T^-$, is then given by the differential equation

$$dN_r/dt = C(a^+ T^+ n + a^- T^- p) , \tag{22}$$

where a^+ (a^-) are the transition probabilities for trapping of an electron (hole) at the negative-U centers, and $C \ll 1$ is the probability that such a trapping event results in the formation of a positive-U center. Since the negative-U defects are believed to be shallow traps near the respective mobility edges, rather than deep recombination centers like the positive-U dangling bonds, the steady-state concentrations n and p of excess carriers, to first order, should be independent of T. This is in agreement with our results in subsection B 2, where the PC has been found to depend only on the density N_r of positive-U dangling bonds. We can, therefore, replace n and p in Eq. (22) by the expressions derived previously [Eq. (8) in the low-intensity regime] and obtain

$$N_r^2(t_{\rm ill}) - N_r^2(0) = 2C[(a^+ T^+ / A_n) + (a^- T^- / A_p)] G t_{\rm ill} . \tag{23}$$

Equation (23) should represent a good approximation as long as N_r is small compared to the density T of negative-U centers. Near saturation ($N_r \approx T$), Eq. (23) has to be replaced by a more complicated expression, however, again with the functional form

$$N_r(t_{\rm ill}) = F(G t_{\rm ill}) . \tag{24}$$

This single dependence of N_r on exposure, Gt, is a consequence of the monomolecular trapping process leading to the metastable defect creation in the negative-U model, in contrast to the bimolecular tail-to-tail recombination in the bond-breaking model.

The kinetic behavior as predicted by Eqs. (23) or (24) for the negative-U model does not explain the available experimental data. We are therefore led to conclude that the correct kinetic description of the SWE is provided by the bond-breaking model as developed above. The implications of this result for the microscopic mechanisms governing the SWE will be discussed in the last section. Before we turn to this topic, however, it is useful to have a closer look at the annealing behavior of the metastable defects.

C. Annealing kinetics of metastable dangling bonds

In the experimental studies of the SWE published so far, relatively little importance has been attached to the annealing of the metastable dangling bonds. Usually the complete disappearance of the reversible changes at elevated temperatures is only mentioned in a semiquantitative manner. However, the kinetics and temperature dependence of the annealing step can be expected to be of similar importance for a detailed understanding of the SWE as the creation of the metastable defects. The more quantitative results known today show that the annealing of the SWE occurs with an activation energy between typ-

ically 0.8 and 1.5 eV, depending on the doping or impurity level of the samples and on the temperature at which the metastable defects have been induced initially.[13,78–80]

The quantity to be examined in a detailed study of the annealing behavior is the number (or density) $N_{\rm ind} = N_s(t) - N_s(0)$ of *induced* spins, rather than the total number of spins, N_s, since the stable dangling bonds, by definition, will not be affected by the annealing procedure. In order to measure $N_{\rm ind}$ as a function of the annealing time for various temperatures, the continuous method as described in Sec. II has been used. Typical raw data obtained on the same sample at increasing annealing temperatures are shown in Fig. 15.

For an interpretation of these experimental results, two simple models are possible. The first of these assumes that the annealing rate $dN_{\rm ind}/dt$ is proportional to the number of existing metastable defects, $N_{\rm ind}$:

$$dN_{\rm ind}(t)/dt = -\nu N_{\rm ind} \ . \tag{25a}$$

This monomolecular annealing mechanism yields, of course, an exponential decay of the metastable dangling bonds with a decay constant ν:

$$N_{\rm ind}(t) = N_{\rm ind}(0)\exp(-\nu t) \ . \tag{25b}$$

Such a monomolecular process is to be expected in the context of the bond-breaking model for the SWE. A different possible annealing process is the bimolecular decay[64] as described by the equations

$$dN_{\rm ind}(t)/dt = -\nu N_{\rm ind}^2 \ , \tag{26a}$$

$$[N_{\rm ind}(t)]^{-1} - [N_{\rm ind}(0)]^{-1} = \nu t \ . \tag{26b}$$

To explain the observed acceleration of the annealing process with increasing annealing temperature T_A, we will assume in this paper, for both the monomolecular and bimolecular models, a thermally activated decay constant,[81]

$$\nu = \nu_0 \exp(-E_a/k_B T_A) \ . \tag{27}$$

The activation energy E_a in Eq. (27) is given by the height V_0 of the energy barrier separating the metastable from the stable state, as depicted schematically in Fig. 1.

In Figs. 16 and 17 we have plotted the raw data for the annealing kinetics according to the monomolecular and bimolecular behavior of Eqs. (25b) and (26b), respectively. In neither of the two methods are the expected straight lines obtained. This indicates that the decay constant ν in Eq. (27) is not a well-defined quantity. Rather, a distribution of activation energies, $P(E_a)$, or of prefactors, $p(\nu_0)$, has to be allowed. Both distributions can be implemented in the configurational model as given in Fig. 1. A distribution of attempt-to-escape frequencies ν_0 can be obtained by different shapes of the total-energy minima in the metastable state, whereas a distribution of activation energies E_a would indicate possible variations in the energy barrier separating the metastable from the stable configuration. In both cases we have to conclude that the metastable configuration is not well defined. This is not surprising in an amorphous material like *a*-Si:H. However, this conclusion has some consequences on the interpretation of the experimental results presented in Figs. 16 and 17. For further analysis we remark that a distribu-

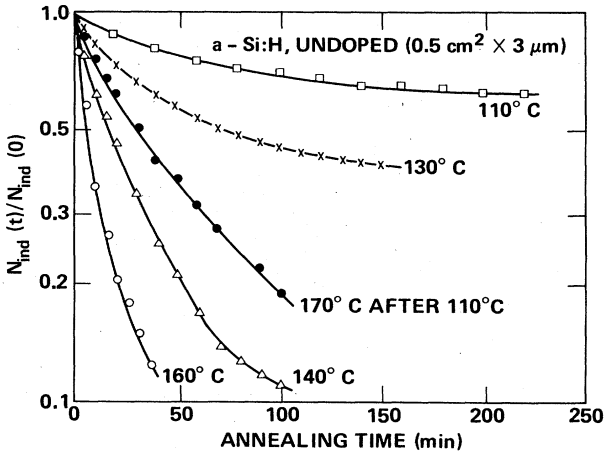

FIG. 16. Annealing of the metastable defects at increasing temperatures plotted according to the monomolecular model [Eq. (25)].

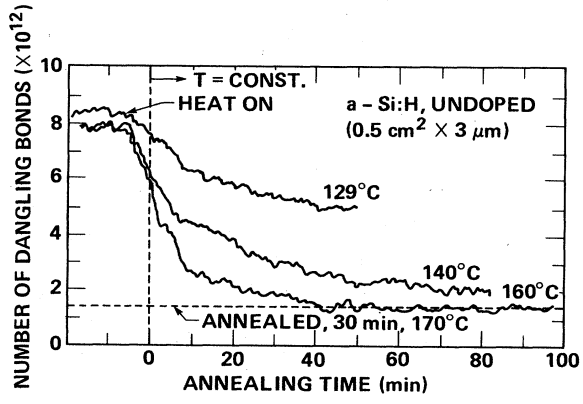

FIG. 15. Decay of the ESR spin signal with annealing time for different annealing temperatures.

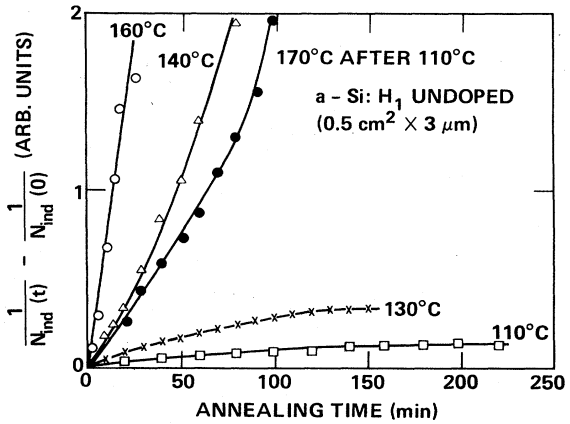

FIG. 17. Same data as in Fig. 16 plotted according to the bimolecular model for the decay of the induced dangling bonds [Eq. (26)].

tion of activation energies will affect the decay constant ν in an exponential way, whereas ν_0 only enters linearly. In the following it will be assumed, therefore, that ν_0 is approximately constant compared to $\exp(-E_a/k_BT_A)$.

Because of the existing distribution of decay rates for the metastable dangling bonds, it cannot be decided directly from Figs. 16 or 17 whether the annealing process is monomolecular or bimolecular. We note, however, that for a monomolecular process according to Eq. (25a) the decay of the *relative* induced spin density, $N_{\rm ind}(t)/N_{\rm ind}(0)$, should be independent of the initial density, $N_{\rm ind}(0)$. In contrast, for a bimolecular mechanism, according to Eq. (26a) the decay of $N_{\rm ind}(t)/N_{\rm ind}(0)$ should slow down significantly with decreasing $N_{\rm ind}(0)$. We have examined the decay of $N_{\rm ind}(t)/N_{\rm ind}(0)$ for two different initial densities, $N_{\rm ind}(0)=3\times10^{16}$ and 1.1×10^{17} cm^{-3}, using the same sample and identical illumination and annealing conditions. The observed decays were in full agreement with the monomolecular behavior in Eqs. (25) and clearly did not follow a bimolecular process.

Therefore, for further analysis we will assume a monomolecular mechanism. Then, the deviation of the experimental curves in Fig. 16 from the expected straight lines yields some information about the distribution $P(E_a)$ of activation energies separating the metastable from the stable SWE state. This information can be extracted using an approximation commonly employed in the analysis of deep-level transient spectroscopy data. After a prolonged illumination, metastable states separated from the ground state by an energy barrier E_a will have become populated by a fraction $N(E_a)=N_{\rm ind}(0)P(E_a)$ of all the created metastable states, $N_{\rm ind}(0)$. The probability distribution $P(E_a)$ is proportional to the density of possible sites with a barrier E_a and the probability of such a state to become occupied during a given illumination procedure. In the following analysis, it is assumed that a metastable state with an energy barrier E_a will have an average lifetime τ given by

$$\tau=1/\nu=1/\nu_0\exp(E_a/k_BT_A)\ . \tag{27'}$$

Here, T_A is the annealing temperature and ν_0 some reasonable attempt-to-escape frequency. We now make the approximation that after an annealing time t all metastable centers with $\tau\le t$, i.e.,

$$E_a\le k_BT_A\ln(\nu_0t)\ ,$$

will have relaxed into the stable ground state. Then the number $N_{\rm ind}(t)$ of remaining metastable states will be given by

$$N_{\rm ind}(t)\approx\int_{k_BT_A\ln(\nu_0t)}^{\infty}N_{\rm ind}(0)P(E_a)dE_a\ . \tag{28}$$

Therefore if we plot $N_{\rm ind}(t)/N_{\rm ind}(0)$ as a function of $k_BT_A\ln(\nu_0t)$, we should obtain the fraction,

$$\int_{k_BT_A\ln(\nu_0t)}^{\infty}P(E_a)dE_a\ ,$$

of metastable states remaining after an annealing time t. Thus, if the illumination conditions are unchanged and the correct value for ν_0 is used, the resulting curves should be independent of the annealing temperature T_A. Alternatively, the magnitude of ν_0 may be determined from the annealing decays by requiring that the different curves coincide when plotted versus $k_BT_A\ln(\nu_0t)$. This is demonstrated in Fig. 18(a), where for the data in Fig. 16 an attempt-to-escape frequency $\nu_0=10^{10}$ s^{-1} has been found, a value that is consistent with frequencies measured for the diffusion of hydrogen in crystalline silicon.

The underlying distribution $P(E_a)$ can now be obtained by taking the derivative of the curves in Fig. 18(a) with respect to $k_BT_A\ln(\nu_0t)$:

$$dN_{\rm ind}(t)/d[k_BT_A\ln(\nu_0t)]=-N_{\rm ind}(0)P(E_a)\ . \tag{29}$$

This leads to Fig. 18(b), showing $P(E_a)$ as a function of energy-barrier height, E_a. The fact that consistent curves are obtained for the whole range of annealing temperatures covered in this study lends further support to the monomolecular annealing mechanism expected for the bond-breaking model for the SWE. The range of activation energies, $E_a=0.9$–1.3 eV, for the annealing of the metastable changes, moreover, is in good agreement with the previously published experimental results. The range of E_a cited here depends weakly on the attempt-to-escape frequency ν_0 used in the analysis. For example, if we use a phonon-like frequency, $\nu_0\approx10^{12}$ s^{-1}, the distribution would be shifted by about 0.2 eV to higher energies, but the curves for different annealing temperatures would not overlap as well.

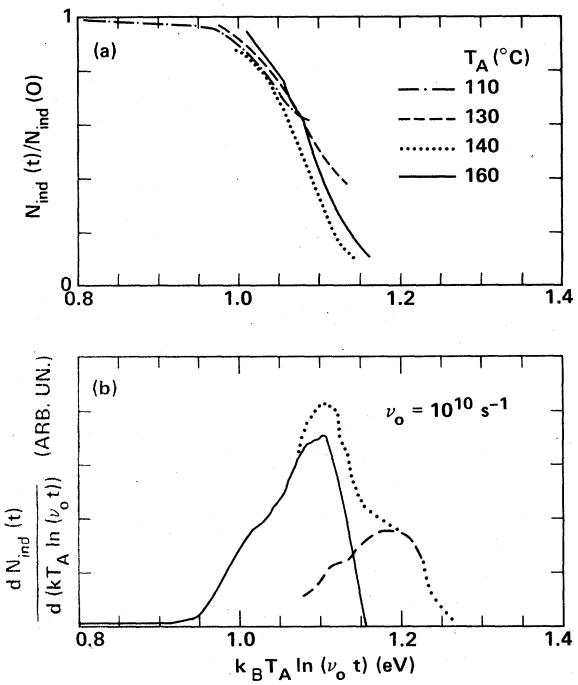

FIG. 18. (a) Fraction $N_{\rm ind}(t)/N_{\rm ind}(0)$ of metastable dangling bonds remaining after an annealing time t as a function of $k_BT_A\ln(\nu_0t)$ for varying annealing temperatures T_A. (b) Distribution of activation energies E_a for the annealing process obtained as the derivative of the curves in (a) (solid line). The dashed curve shows the distribution of activation energies remaining after a preceding low-temperature anneal. The dotted line is the sum of these two distributions.

This concept of a distribution of possible decay constants ν can be tested further by performing the following two-step experiment. After prolonged illumination, a sample is first annealed at a low temperature (110 °C) for a sufficiently long time. If initially a distribution of activation energies E_a has been present for the sample, this low-temperature anneal should heal all the metastable defects with sufficiently small activation energies, but should leave all defects with larger activation energies E_a unaffected. The net result of a preceding low-temperature anneal is, therefore, a narrowing of the distribution $P(E_a)$ and a shift of the average activation energy $\langle E_a \rangle$ toward larger values. Thus, a following high-temperature anneal should exhibit a more exponential and slower decay of N_{ind} than the same annealing process without a preceding low-temperature anneal. Both effects are observed for the curve marked "170 °C after 110 °C" in Fig. 16. The distribution $P(E_a)$ remaining after the low-temperature anneal is shown by the dashed line in Fig. 18(b). This confirms our earlier conclusion that, indeed, the metastable state in the SWE is not well defined, but that rather a fairly wide distribution of metastable dangling-bond states exist. This experimental result is consistent with the fact that the stable dangling-bond defect in a-Si:H, too, is not well defined, but subject to environmental variations. Finally, it seems likely that, as a consequence of the existing distribution, the identification of the metastable defect(s) causing the SWE will remain, to some extent, ambiguous.

D. The influence of other external parameters: Photon energy and illumination temperature

In this section we will present experimental results concerning the influence of two other external parameters on the kinetic behavior of the SWE. These parameters are the energy $h\nu$ of the photons used for the illumination of the a-Si:H samples and the temperature T at which this illumination occurs. We will first discuss the influence of the photon energy $h\nu$. In determining the dependence of the metastable changes on $h\nu$, special care has to be taken to correctly account for the large changes in the generation rate G that result from the strong dependence of the absorption on $h\nu$. The following discussion can be based on Eq. (21) (see subsection B 2). This equation states that in the limit of low total exposure the dependence of the PC on illumination time can be written as

$$[1/\sigma_{\text{ph}}(0)]\{[1/\sigma_{\text{ph}}(t_{\text{ill}})]-[1/\sigma_{\text{ph}}(0)]\} \propto c_{\text{SW}} t_{\text{ill}} \ . \qquad (21')$$

Note especially that the right-hand side of this expression is independent of the generation rate G, so that any complications due to changes of G as mentioned above can be avoided. Moreover, for these experiments, the intensity of the monochromatic illumination was adjusted to always give approximately the same initial value $\sigma_{\text{ph}}(0)$ of the PC, and was kept low enough to make Eq. (21') a valid expression. If one then plots the photoconductivity data accordingly, straight lines with a slope proportional to the defect-creation efficiency c_{SW} are to be expected. Typical experimental curves are shown in Fig. 19. The inset in this figure summarizes the dependence of the slope of the straight lines and therefore of the defect-creation efficiency as a function of the photon energy between $h\nu = 2.1$ and 1.2 eV. The data points are average values obtained from a variety of runs such as shown in Fig. 19. Below 1.2 eV no metastable changes in the PC could be induced with the available light sources even after illumination for longer than 8 h. These experiments show that the efficiency for creating metastable dangling bonds is, within the experimental accuracy of about 50%, independent of the photon energy down to $h\nu = 1.2$ eV. At first sight this result is surprising, since intuitively one would expect high-energy photons to be much more effective in creating structural changes than sub-band-gap photons. However, one has to keep in mind that the radiative tail-to-tail recombination in a-Si:H occurs with a luminescence energy of about 1.2 to 1.3 eV, independent of the exciting photon energy.[82] The explanation for this experimental fact is based on the assumption that photoexcited carriers first lose energy in excess of the tail separation (≈ 1.3 eV) by a multiphonon thermalization process and/or by a possible Stokes shift during recombination. In the case of the nonradiative tail-to-tail recombination events responsible for the metastable defect creation, similar energy losses are likely to occur prior to the final, defect-inducing transition. This, then, would provide a natural explanation for the missing influence of $h\nu$ on the magnitude of the SWE.

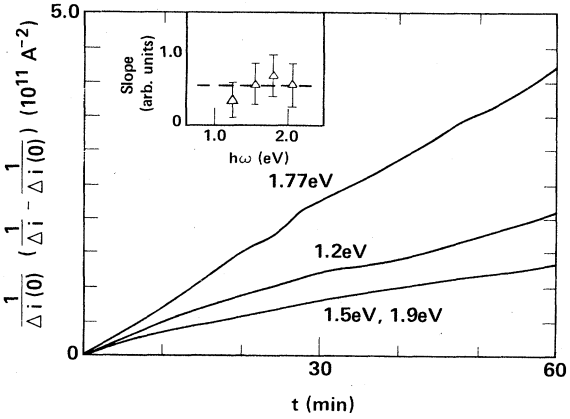

FIG. 19. Dependence of the defect-creation efficiency on the photon energy. The experimental results have been plotted according to Eq. (21) for photon energies between 1.2 and 2.1 eV. The inset shows the slopes of the obtained straight lines as a function of photon energy.

For the discussion of the second parameter, i.e., the temperature T at which the illumination takes place, it is useful to divide the range of temperatures into two regions. The first region is that of $T \lesssim 90$ °C, for which it is possible to neglect the effects of simultaneous annealing of the light-induced defects on the kinetic behavior for short times. The increase of the ESR signal due to metastable dangling bonds in this regime is shown in Fig. 20(a) for three different temperatures. Again the $t^{1/3}$ dependence on illumination time is observed as soon as $N_s(t) \geq 2N_s(0)$ (cf. Fig. 6). However, the spin density measured at a given time increases slightly with increasing temperature. More precisely, the inset in Fig. 20(a) shows

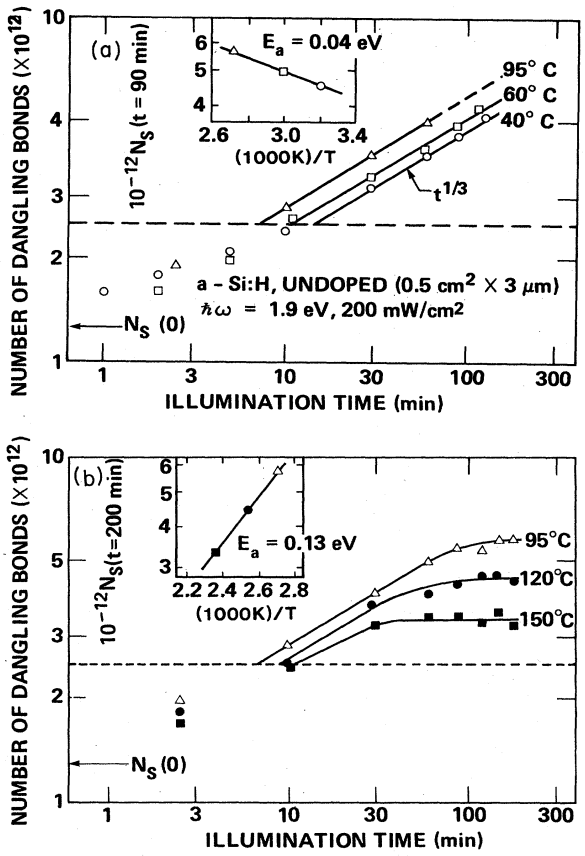

FIG. 20. (a) Temperature dependence of the defect creation in the low-temperature regime. The inset shows that the creation is thermally activated with an energy of 0.04 eV. (b) Saturation of the ESR spin density for different illumination temperatures. According to the inset the saturation level is thermally activated with $E_a = 0.13$ eV.

that the obtainable spin density in the $t^{1/3}$ regime is thermally activated with an activation energy of 0.04 eV. This result agrees quantitatively with previous measurements by Pankove and Berkeyheiser[8] and by Dersch.[63] We can easily implement this experimental fact into the kinetic theory by assuming the efficiency constant c_{SW} to be thermally activated according to

$$c_{SW}(T) = c_{SW}(0)\exp[(-0.04\text{ eV})/k_BT)] . \quad (30)$$

The physical reason for Eq. (30) is still not clear. We would like to comment, however, that the same activation energy has been reported for the $\mu\tau$ product of electrons in a-Si:H,[83] and that a similar energy describes the exponential decay of the tail states in a-Si:H.[84] One possible explanation of Eq. (30), for example, could be the decrease of the thermalization depth of photoexcited carriers with increasing temperature due to thermal reemission into higher tail states. A different mechanism could involve an increase of the probability of excess carriers to recombine at sites more susceptible for photostructural changes, because of the changes in the lifetime-mobility product.

The defect creation for illumination in the high-temperature regime, $T > 90$ °C, is characterized by the saturation of the ESR spin density at a constant value seen in Fig. 20(b). As evident from the strong temperature dependence of this saturated spin density, the steady-state condition is given by a detailed balance between the rate of light-induced dangling-bond creation and the thermal annealing rate. For an approximate qualitative analysis, we can combine Eqs. (11′), (25a), (27), and (30) to yield the following differential equation that combines both creation and annealing of the metastable defects together with the adequate temperature dependence:

$$dN_s/dt = C\exp[(-0.04\text{ eV}/k_BT)](G/N_s)^2 - \exp(-E_a/k_BT)[N_s - N_s(0)] . \quad (31)$$

The long-time limit of the spin density, N_{stat}, follows from the steady-state condition $dN_s/dt = 0$ as

$$N_{stat}^2[N_{stat} - N(0)] = CG^2\exp[(E_a - 0.04\text{ eV})/k_BT] . \quad (32)$$

To the extent that $N_{stat} \gg N(0)$ and $E_a \gg 0.04$ eV, Eq. (32) can be approximated by

$$N_{stat} \propto G^{2/3}\exp(E_a/3k_BT) . \quad (32')$$

The inset of Fig. 20(b) shows an experimental value of 0.13 eV for $E_a/3$. The resulting $E_a = 0.4$ eV is significantly smaller than the range $0.9 \leq E_a \leq 1.3$ eV obtained in subsection C. Apart from the limited validity of the approximations leading to Eq. (32′), the reason for this discrepancy can be sought in Eq. (31), where we have combined rates for processes occurring at thermal equilibrium (annealing) with those for processes requiring large deviations from thermal equilibrium (defect creation). Nevertheless, the present description agrees at least qualitatively with the overall kinetic model for the SWE in this paper.

We would like to finish this section by briefly commenting on the question concerning the saturation of the SWE. The first comment is that the strongly sublinear time dependence ($t^{1/3}$) of the defect creation can easily be mistaken for an approach towards a limiting value when plotted on a linear timescale. For example, according to Fig. 6 it takes about 5 h of 400-mW/cm² illumination to increase the spin density in undoped a-Si:H from 2×10^{16} to 6×10^{16} cm^{-3}. Following the $t^{1/3}$ time dependence, it would take about 2 d of the same illumination to reach a density of 2×10^{17} cm^{-3}, and nearly one year for a defect density of 1×10^{18} cm^{-3}.

A real saturation of the effect will be observed in two cases. At high enough temperatures saturation occurs when creation and annealing rates become comparable, as discussed above. The second, more interesting case is that of saturation due to the depletion of accessible metastable sites, since this could yield additional information about the microscopic origin of the SWE. However, we do not know of any study in which a metastable defect density larger than 10^{18} cm^3 has been reported for undoped amorphous silicon. Typical increases of the dangling-bond density in undoped a-Si:H are of the order of 10^{17} cm^{-3}. Most likely these numbers do not reflect the depletion of metastable states, but rather kinetic limitations as dis-

cussed in this paper. In order to better establish the maximum density of metastable dangling bonds possible in *a*-Si:H, a long-time experiment under carefully controlled temperature conditions would be necessary.

E. The microscopic origin of the Staebler-Wronski effect

So far we have given a description of the SWE in macroscopic, phenomenological terms. In this last subsection we use our experimental results to speculate on possible microscopic mechanisms responsible for the reversible defect creation in *a*-Si:H. However, as our present knowledge about the microscopic structure of amorphous silicon is still very limited, so is our understanding of structural *changes* in this material. This can be regarded as the main reason why, despite the extensive experimental efforts, no conclusive picture of the SWE has emerged so far. Even basic questions are still the subject of controversial discussion, e.g., whether the SWE is caused by impurities, whether one or more species of metastable defects exist, or whether actually new defects are caused at all during illumination, rather than the charge state of already existing defects being changed by predominantly electronic processes. At the beginning of this discussion, it is therefore useful to clearly state our answer to these questions, as we think it follows from the experimental results presented here:

The SWE in pure, undoped *a*-Si:H is caused by the self-limiting creation of dangling-bond-like defect states, resulting from the breaking of bonds intrinsic to the amorphous network.

This statement contains four major points that need further elaboration.

(1) Our conclusion that the SWE is intrinsic to the *a*-Si network, as opposed to an impurity related origin, is based on the results presented in subsection A. There it was demonstrated that the magnitude of the SWE is constant over 2—3 orders of magnitude in impurity concentration, once a critical value of [O],[N] $< 10^{19}$—10^{20} cm^{-3} has been achieved. Further below we will discuss the creation of metastable defects on the basis of the breaking of weak Si—Si bonds. Such bonds exist in *a*-Si:H with an intrinsic density of about 10^{18}—10^{19} cm^{-3}. A plausible explanation for the critical impurity concentrations cited above is, therefore, given by the condition that the density of impurity-related bonding configurations susceptible to (or enhancing) light-induced dangling-bond creation has to be significantly larger than the density of intrinsic sites derived from strained Si—Si bonds, before the SWE will be dominated by the impurity-derived sites. This implies also that the magnitude and kinetic behavior of the SWE can be expected to be different in the case of large impurity contents, in accordance with the experimental evidence. In particular, the activation energy of the annealing step is found to drop significantly with increasing impurity content.[41,42] In this sense, the SWE is an intrinsic phenomenon, but is enhanced by the presence of high impurity concentrations.

(2) The self-limiting character of the SWE is caused by the fact that the defect-inducing step, i.e., the nonradiative tail-to-tail recombination, is quenched by the previously induced metastable defects. This specific property leads to the characteristic sublinearity ($I^{2/3}t^{1/3}$) of the SWE in light exposure and is a natural consequence of a microscopic process based on bond breaking via tail-to-tail recombination. In contrast, rather stringent assumptions have to be made in order to fit the observed behavior to other microscopic models (cf. discussion in subsection B 4).

(3) The main metastable defect state is the silicon dangling bond. Here, the comment we would like to make concerns the work "main." To a large extent the experimental results in this study are based on ESR measurements. In this case, the only significant defect state near midgap detected is the neutral dangling bond, D^0. On the other hand, the dangling-bond state is known to dominate the optoelectronic properties of undoped *a*-Si:H. Since the photoconductivity is especially sensitive to any change in the density of deep defect levels, it is safe to conclude from the quantitative agreement between the analysis of the ESR intensity and the PC in subsection B 3 that metastable changes other than those of the dangling-bond density have relatively little influence on the macroscopic properties of undoped *a*-Si:H. Furthermore, one has to keep in mind that the dangling-bond defect in *a*-Si:H is by no means well defined. A broad distribution (width 0.2—0.3 eV) of defect states in amorphous silicon is referred to by this name. It is conceivable that different experiments will weigh this distribution or changes in it differently, giving rise to some ambiguity as far as the position of the defect states in the gap causing the metastable changes is concerned. The present situation can best be summarized by saying that there is no forcing evidence for the existence of defect states other than dangling bonds, but that the presence of such states at lower densities can not be excluded.

(4) The last point to discuss is whether prolonged illumination leads to the creation of new dangling bonds by bond breaking, or whether preexisting negative-U centers ($D^+ + D^-$) are transformed into neutral dangling bonds by preferential capture of excess electrons or holes. Both assumptions would, in principle, explain the increase in the density N^0 of neutral dangling bonds, which is one of the few experimental facts established beyond any doubt so far. However, the bond-breaking model is capable of explaining a variety of experimental results that are inconsistent with or difficult to understand in the context of the negative-U model. We have already mentioned the explanation of the kinetic behavior of the SWE, which emerges naturally from the bond-breaking model, but is in qualitative disagreement with the negative-U model. A second point is that the SWE is generally not observed in materials with dangling-bond densities in excess of 10^{18} cm^{-3}, like *a*-Ge:H or high-defect-density *a*-Si.[85—87] Again, in the context of the bond-breaking model these experimental results are easily explained. The large number of dangling bonds already existing in these materials shorts out any direct recombination events very effectively. So, the $t^{1/3}$ dependence derived in subsection B 1 predicts that it would take of the order of five years (!) of intense illumination (0.5 W/cm^2) to increase the spin density of *a*-Si:H from 1×10^{18} to 2×10^{18} cm^{-3}. On the oth-

er hand, the density of negative-U dangling-bond centers should increase in a manner similar to the concentration of positive-U dangling bonds. Moreover, the defect-creation rate in the negative-U model is much less dependent on the density of recombination centers, N_r [cf. Eq. (22)]. Thus, one would expect a noticeable SWE in samples with higher defect densities, which is clearly not observed.

Some support for the negative-U model has been drawn from a conjecture by Dersch *et al.*[11] that the metastable dangling bonds created during the illumination must be separated by a distance of more than 10 Å, in order to avoid changes in the ESR line shape (exchange narrowing) not seen experimentally. Dersch and co-workers used the observation of similar line shapes for the stable and metastable dangling bonds to argue that the dangling-bond pairs created by Si—Si bond breaking have to become spatially separated on the basis of hydrogen diffusion. However, macroscopic diffusion of hydrogen in a-Si:H is known to be activated with an energy of 1.5 eV,[88,89] a value that is incompatible with the small activation energy (0.04 eV) of the SWE (see subsection D). In the negative-U model, on the other hand, separation of metastable dangling bonds can be achieved fairly easily, since only electronic diffusion is required. Thus, the notion that the metastable dangling bonds have to be spatially separated to avoid exchange narrowing of the ESR signal has been regarded as an important point in favor of the negative-U model.

However, in a strongly disordered material like a-Si:H the interpretation of the ESR line shape is not so straightforward. Here the linewidth ΔH_{pp} of the dangling-bond signal is determined by the convolution of two distributions.[84] The first component, the powder pattern, arises from the random orientation of the dangling-bond symmetry axis with respect to the external magnetic field in any macroscopically isotropic material. The second component, the environmental broadening, reflects the fact that even dangling bonds with the same orientation will still couple to slightly different crystal fields because of the missing long-range order in a-Si:H. Exchange narrowing, then, results from the spatial overlap of the wave functions of neighboring spin states, leading to an averaging of the random orientations and fluctuating environments. In amorphous silicon this is observed by a decrease of the ESR linewidth from typically 8 to 4 G, when the spin density is larger than 10^{18}–10^{19} cm^{-3}, depending somewhat on the homogeneity of the spin distribution.[90] For the low spin densities encountered in good a-Si:H films (10^{16} cm^{-3}) the dangling bonds can be regarded as spatially isolated and, therefore, the ESR linewidth reflects the full disorder of the material. Now, in the bond-breaking model of the SWE, closely related pairs of metastable dangling bonds are created. This could, in principle, lead to observable effects on the ESR line shape, due to the strong interactions between the two spins in each pair, as proposed by Dersch *et al.*, but the exchange interaction occurring inside each of these pairs is not sufficient to produce an exchange narrowing of the whole ESR line. For such a narrowing it is essential that a large number of spins occupying a reasonably large portion of the amorphous sample interact strongly with each other.[90] In all other cases no drastic effect on an inhomogeneous resonance spectrum is to be expected. If we consider, for example, a system of close pairs of dangling bonds, each of which is isolated from the neighboring pairs, the situation will be very similar to that of a dilute spin system, as long as no diamagnetic spin pairing occurs. The system of isolated spin pairs will be affected by the broadening due to orientational and environmental disorder in much the same way as a system of isolated single spins would be. As a consequence, contrary to the earlier conjecture, the creation of metastable dangling bonds by bond breaking is not at variance with the similarity between the ESR signals obtained for stable and metastable defects and does not require any subsequent separation of pairs. Considering all this, we feel that the experimental evidence favors the bond-breaking model of the SWE over the negative-U model.

The question concerning the microscopic origin of the SWE is then reduced to finding atomic configurations that allow the metastable formation of dangling bonds in accordance with the existing experimental data. Since the effect seems to be intrinsic to the pure a-Si:H network (cf. subsection A), it can only involve the breaking of Si—H or Si—Si bonds. The first alternative, i.e., Si—H bond separation, seems unlikely because of energy considerations. Breaking of the Si—H bond requires an energy of about 3.5 eV,[89] and can occur when a-Si:H is irradiated with energetic particles[91] or when the material is annealed at temperatures above 400 °C.[89,92] In the first case enough energy is available to actually create dangling bonds and interstitial atomic hydrogen. Both defects can be detected by ESR after the irradiation.[91] However, a similar process is very unlikely to be caused by illumination with low-energy photons, $h\nu < 3$ eV. Furthermore, no ESR signal due to atomic hydrogen has been observed in the light-soaked state.[86] In the case of Si—H bond breaking by annealing, the process is made possible by the enhanced mobility of atomic hydrogen in a-Si at high temperatures. Then, the energy needed to break a Si—H bond can be recovered by the formation of H_2 molecules. This buildup of molecular hydrogen in a-Si:H has recently been detected in a variety of experiments.[93–96] For an explanation of the SWE, however, a similar mechanism is not possible, since it would lead very quickly to irreversible light-induced changes.

So the most probable microscopic explanation for the SWE is that of Si—Si bond breaking. This process has already been proposed in several versions by a number of authors (e.g., Refs. 8, 11, 13, 22, 37, 39, 97, and 98). An important question unanswered until now is whether local rearrangements of hydrogen atoms are necessary to explain the observed metastability of the light-induced defects, or whether structural relaxation of silicon atoms alone is sufficient. A solution to this problem could be obtained, for example, by theoretically calculating energy-configuration diagrams like the one in Fig. 1 for various simple atomic configurations likely to occur in hydrogenated amorphous silicon, and then comparing the obtained potential barriers V_0 and energy differences ΔE with their experimental values.

We would like to give an example of *one* possible microscopic mechanism for the SWE. Figure 21 shows an atomic configuration that should be fairly common in *a*-Si:H. In the annealed state, *A*, the atomic arrangement is that of a weak Si—Si bond with a hydrogen atom bonded by at least one of the three remaining "backbonds" of one of the two silicon atoms forming the weak bond. Since the hydrogen concentration in *a*-Si:H is typically of the order of 10 at.%, statistically every fifth weak bond would exist in such a configuration. Therefore, in pure *a*-Si:H about 10^{18} cm^{-3} atomic clusters like the one shown in Fig. 21(a) should be present.

Under steady-state illimination, holes will be trapped preferentially by the weak Si—Si bonding states. Trapping of a hole will lead to further weakening of the Si—Si bond, since an electron has been optically excited out of a bonding orbital. Depending on the initial distance and/or bond angle of the two silicon atoms forming the weak bond, this bond could actually break after the hole-trapping event because of the attractive forces exerted by the backbonds. The hole trapping would thus give rise to a reconstruction of the form $Si—Si \leftrightarrow D^0+D^++e^-$, i.e., to dangling-bond formation without hydrogen being directly involved in the process. Whether this would actually lead to metastable dangling bonds that are separated from the ground state (i.e., the original weak bond) by an energy barrier of about 1 eV has to be decided by model calculations.

The preceding scenario might be possible for a small number of sufficiently weak bonds. The observation of a stable hole resonance by light-induced ESR or ESR measurements in undoped and boron-doped *a*-Si:H samples shows, however, that for the majority of the weak Si—Si bonds trapping of an optically excited hole does not lead to bond breaking.[99] For these bonds the additional vibrational energy set free by a nonradiative direct electron-hole recombination is necessary to break the weak bond. This additional energy will be available in the form of local Si—Si and Si—H phonon modes, depending on the specific electron-phonon coupling of the cluster in Fig. 21(a). Once this local vibrational energy has dissipated the weak bond can reform, and no formation of metastable dangling bonds would have resulted. This reformation of the bond can be prevented by the presence of an additional atomic rearrangement acting as a stabilizing process. This additional process could, for example, involve the switching of the backbonded hydrogen atom into the broken weak bond, as shown in Fig. 21(b), and would be favored by the fact that the Si—H vibrational energy is about 4 times larger than that of the Si—Si bond, so that only a relatively small number (6) of Si—H phonons have to be emitted. Moreover, the switching of the Si—H bond requires much less energy than 3 eV, because the bond is never actually broken. As indicated in Fig. 21(b), this process would result in the formation of two silicon dangling bonds, or one dangling bond plus a Si—H—Si hybrid state. For both processes presented here the reversibility by annealing is evident, since only local atomic reconfigurations are required.

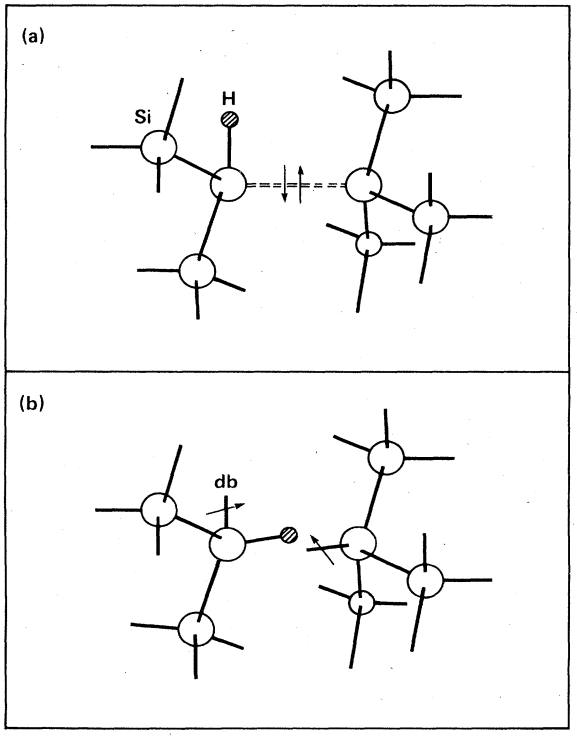

FIG. 21. A possible microscopic process leading to the creation of metastable dangling bonds. See text for a discussion.

It is worthwhile to consider the characteristic energies (cf. Fig. 1) involved in a process like the one presented in Fig. 21 in comparison with the experimental results discussed previously. These energies are the recombination energy E_R available for the formation of metastable states, the energy barrier V_0 that has to be overcome for transitions between the stable and metastable state, and the energy difference ΔE between these states. For photon energies $h\nu$ larger than the band gap, $E_g \approx 1.9$ eV, one can write $E_R = h\nu - E_{\text{th}}$, where E_{th} is the thermalization energy lost by an electron-hole pair prior to the defect-inducing recombination event. For lower-energy photons, $h\nu < E_g$, two absorption events may be necessary to form an electron-hole pair capable of defect creation, so that $E_R = 2h\nu - E_{\text{th}}$. We can combine these two cases to a good approximation by letting $E_R = E_g - E_{\text{th}}$. As far as V_0 is concerned, the annealing results in subsection C suggest quite conclusively values around $V_0 = 1.1 \pm 0.2$ eV. Note that this is similar to the activation energy for hydrogen diffusion in *a*-Si:H (Refs. 11 and 13, and references therein). This lends some support to a microscopic process like the one in Fig. 21, since the bond-switching motion of the hydrogen atom can be regarded as the elementary step for the long-range diffusion of hydrogen in the Si network. To obtain an estimate for ΔE, we first consider the increase in electronic energy resulting from the promotion of two electrons out of a weak Si—Si bonding state into a singly occupied dangling-bond state. Assuming a width of about 0.3 eV for the valence-band tail and a 0.2-eV-wide dangling-bond band centered slightly below midgap, this gives a possible range of ΔE between 2×0.3 and 2×0.7 eV. In addition to this purely electronic energy, one has to allow for a certain degree of

structural relaxation, E_{rel}, so that finally $\Delta E = (0.6-1.4$ eV$) - E_{rel}$. According to the static potential-energy diagram in Fig. 1, the recombination-induced creation of metastable dangling bonds becomes possible for all transitions with $E_R > V_0 + \Delta E$. Using the values estimated above, there will be a reasonable range of initial and final states satisfying this inequality, provided that the thermalization losses E_{th} are small enough and/or the energy gain by structural relaxation, E_{rel} is large enough. From this standpoint, then, the process shown in Fig. 21 would be energetically possible. On the other hand, one can envisage a more unfavorable situation, with thermalization into deep tail states, giving $E_R \approx 1.4$ eV, and no energy gain by relaxation. Then, for most cases, E_R will be, by about 1 eV, smaller than $V_0 + \Delta E$, and, consequently, transitions into the metastable state would appear impossible. However, this is not necessarily true. The argument is that the value for the energy barrier V_0 has been measured by annealing of the metastable states, i.e., V_0 constitutes the barrier for thermal transitions between the metastable and the stable states. It is *a priori* not clear whether the same value applies to the strongly localized, nonequilibrium creation event, or whether in the case of the local excitation the energy barrier for the transition between the two states can be effectively lower. A more detailed investigation of this question is desirable but beyond the scope of this paper.

A final remark concerns the source of the energy E_R driving the creation of the metastable dangling bonds. Experimental support exists for the trapping- and the recombination-induced origin of the SWE. As far as the mechanism caused by nonradiative recombination is concerned, it has been the basis for the explanation of our experimental data. In the case of the trapping-related origin of the SWE, evidence comes from the fact that the small metastable changes can be induced by current soaking of *p-i-p* structures[36,100] without illumination. However, the interpretation of these experimental results has to be taken with some caution, since the occurrence of recombination due to double-carrier injection and/or thermal exitation cannot be excluded with certainty.

IV. CONCLUSIONS

We have undertaken a systematic study of the Staebler-Wronski effect (SWE) in undoped hydrogenated amorphous silicon, using electron-spin-resonance and photoconductivity measurements. The influence of impurity concentration, sample thickness, illumination time and intensity, photon energy, and temperature on the creation of metastable defects as well as the variation of the annealing behavior with annealing temperature has been studied in detail. The results of this study can be summarized as follows:

(1) The SWE is intrinsic to hydrogenated amorphous silicon and does not depend on the concentration of the major impurities, nitrogen and oxygen, below a critical value of about 10^{19} cm^{-3}. For higher impurity contents an enhancement of the metastable changes with increasing N or O concentration is observed.

(2) The SWE is a bulk effect. However, the probability of creating metastable defects is, by about 1 order of magnitude, larger in a surface/interface layer with a total thickness of about 0.5 μm than in the rest of a sample. Possible reasons for this inhomogeneity are the existence of band bending and/or mechanical stress near the surface or interface.

(3) The kinetic behavior of the metastable dangling-bond density and of the photoconductivity, i.e., the dependence of these quantities on illumination time t_{ill} and light intensity I, can be described quantitatively by a model based on the nonradiative direct tail-to-tail recombination of optically excited electrons and holes. The kinetic behavior is sublinear in total exposure, It_{ill}. For example, at long times the dangling-bond density increases as $I^{2/3}t_{ill}^{1/3}$. The physical reason for this functional dependence of the spin density on the kinetic parameters is the major role of the dangling bonds as recombination centers in *a*-Si:H. This results in a self-limiting character of the SWE, confining the densities of metastable dangling bonds to typically 10^{17} cm^{-3}. Moreover, the comparison of the metastable changes observed in the ESR spin density and the photoconductivity shows that the predominant metastable defect caused by prolonged illumination is the silicon dangling bond, at least as far as the optoelectronic properties of *a*-Si:H are concerned.

(4) The annealing behavior of the metastable defects can be described consistently by a monomolecular, exponential decay with a thermally activated decay constant. The activation energy of this decay constant is not well defined. A distribution of activation energies between 0.9 and 1.3 eV is obtained from the annealing experiments. This shows that the metastable dangling bond is subject to local variations.

(5) The efficiency for the creation of metastable defects is found to be independent of the photon energy $h\nu$ in the range $h\nu = 1.2-2.1$ eV. This suggests that the defect-inducing step, like the radiative, luminescent recombination, occurs after thermalization of the optically excited carriers into deep tail states. Consistent with previous experimental results, the defect-creation rate is found to be thermally activated with a small energy of 0.04 eV. Together with the results summarized in point (4), this allows the determination of the steady-state defect density reached asymptotically under illumination at elevated temperatures.

(6) Our experimental data are consistent with a microscopic model of the SWE based on the breaking of weak Si—Si bonds, in contrast to the negative-U model, which postulates the capture of excess electrons and holes as the origin of the SWE. Moreover, it seems likely that the complete microscopic mechanism involves the reconfiguration of Si—H bonds as a stabilizing element.

ACKNOWLEDGMENTS

We would like to thank R. A. Street and D. K. Biegelsen for stimulating and clarifying discussions. This study was supported by the Solar Energy Research Institute (Golden, Colorado) under Contract No. XB-3-03112-1.

APPENDIX: OCCUPANCY OF THE DIFFERENT CHARGE STATES OF DANGLING BONDS IN *a*-Si:H DURING ILLUMINATION

The recombination scheme for *a*-Si:H based on the detailed balance between the possible transitions in the assumed quasi-steady-state conditions during illumination (Sec. III B 1) can be used to determine the relative occupancies $n^+=N^+/N_r$, $n^0=N^0/N_r$, and $n^-=N^-/N_r$ of the different dangling-bond charge states (D^+, D^0, and D^-). Here the total number (or spatial density), N_r, of dangling bonds is given by

$$N^+ + N^0 + N^- = N_r \ . \tag{A1}$$

Moreover, we obtain, from Eqs. (3a)—(3e) in the quasi-steady-state approximation,

$$A_n^0 N^0 + A_n^+ N^+ = G/n - A_t p \ , \tag{A2}$$

$$A_p^- N^- / A_n^0 N^0 = n/p \ , \tag{A3}$$

$$(A_p^- N^- - A_p^0 N^0)/(A_n^0 N^0 - A_n^+ N^+) = n/p \ , \tag{A4}$$

$$A_p^0 N^0 / A_n^+ N^+ = n/p \ , \tag{A5}$$

$$A_p^0 N^0 + A_p^- N^- = G/p - A_t n \ . \tag{A6}$$

Finally, charge neutrality gives the additional condition

$$n + N^- = p + N^+ \ . \tag{A7}$$

A detailed solution of this system of coupled equations is only possible numerically, and the quantitative results are not very meaningful because of the large number of only approximately known transition probabilities involved. We will, therefore, use a more qualitative picture, which is, however, sufficient to provide the necessary information about the relative occupancies n^+, n^0, and n^- of the dangling-bond states used in Sec. III B 1.

First of all, Eqs. (A3) and (A5) can be combined to give a law-of-mass-action relation:

$$(N^0)^2/(N^+N^-) = (A_p^- A_n^+)/(A_p^0 A_n^0) = \beta \ . \tag{A8}$$

This relationship links the ratio of neutral and charged dangling bonds to the ratio β of the relevant cross sections for excess carrier capture. [The same result follows from the combination of Eqs. (A2), (A4), and (A6).] Equation (A8) can be combined with Eq. (A1) to yield the allowed occupancies n^+, n^0, and n^- compatible with the recombination model of Fig. 4:

$$n^{\pm} = \tfrac{1}{2}(1-n^0) \mp [\tfrac{1}{4}(1-n^0)^2 - (n^0)^2/\beta]^{1/2} \ . \tag{A9}$$

The corresponding "phase diagram" for n^+, n^0, and n^- is shown in Fig. 22 for a value of $\beta=15$. The maximum proportion $n^0_{\max}$ of neutral dangling bonds is given by

$$n^0_{\max} = \beta^{1/2}/(2+\beta^{1/2}) \ . \tag{A10}$$

According to (A3)—(A5), the ratio n/p of excited electrons and holes is the parameter determining at which point of Fig. 22 the system will be for a given generation rate G and total dangling-bond density N_r.

So far, our analysis is exact. To proceed further, however, we will need some information about the transition

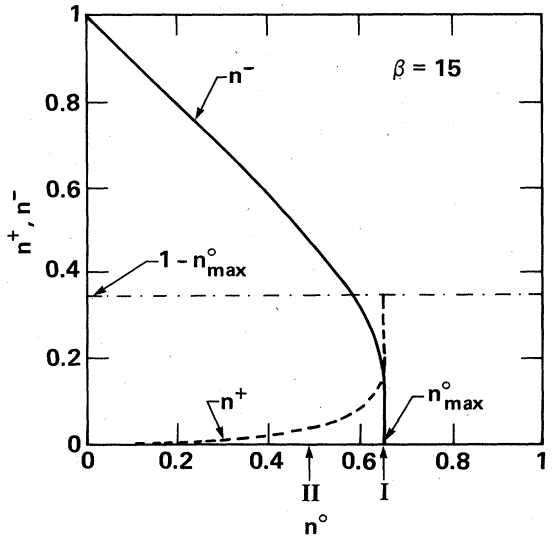

FIG. 22. Phase diagram for the different dangling-bond charge states under illumination. n^0, n^+, and n^- are the fractions of neutral, positively, and negatively charged dangling bonds. I and II refer to the cases of weak and strong illumination, respectively.

probabilities A_p^-, A_p^0, A_n^0, and A_n^+ of the optically excited electrons and holes. This is necessary, for example, to decide which one of the two branches in Eq. (A9) should be assigned to n^+ and which to n^-. It can be expected that the transition probabilities A_p^- and A_n^+ for the charged carriers into oppositely charged dangling bonds will be larger than the probabilities A_p^0 and A_n^0 for transitions into neutral states. A quantitative estimate for the different transition probabilities can be deduced from recent time-of-flight measurements by Street.[73] Approximate values for room temperature are compiled in Table I. From these numbers one can deduce a value of $\beta \approx 15$, as used in Fig. 22.

We are now able to derive the relative occupancies n^+, n^0, and n^- of the dangling bonds for the following two limiting cases.

1. Case I: Weak illumination ($n,p \ll N_r$)

This is the case of very small, but nevertheless nonzero, concentrations of excited carriers n and p. $n,p \neq 0$ is necessary to make sure that Eqs. (A3) and (A5) are mean-

TABLE I. Approximate values of the room-temperature transition probabilities for capture of electrons and holes in *a*-Si:H by different charge states of dangling bonds. (Probabilities are given per volume density of initial and final states.)

Symbol	Transition	Probability (10^{-9} cm^{3}s^{-1})
A_p^0	$h+D^0 \rightarrow D^+$	0.7
A_p^-	$h+D^- \rightarrow D^0$	2
A_n^0	$e+D^0 \rightarrow D^-$	2
A_n^+	$e+D^+ \rightarrow D^0$	10

ingful and not singular. This can be achieved by weak steady-state illumination or, perhaps, already by the small number of thermally excited carriers at room temperature. Equation (A10) implies that under these conditions $(n,p\neq 0)$ at least $N_r(1-n^0_{\max})$ dangling bonds will be charged. For the value of $\beta\approx 15$ given above, the fraction of charged bonds is at least $n^-+n^+\geq 1-n^0_{\max}\approx\frac{1}{3}$. Note that the value of $n^0_{\max}$ only depends on the different transition probabilities and, in particular, is independent of the generation rate G. It is, therefore, always possible to choose an illumination intensity low enough so that $\max(n,p)\ll N_r(1-n^0_{\max})$. In this weak-illumination case, the neutrality condition (A7) can only be satisfied if $N^-\approx N^+$ $(n^-\approx n^+)$. The only region in the phase diagram of Fig. 22 satisfying this condition is the region near $n^0=n^0_{\max}$. The occupancy in the weak-illumination case is therefore given by

$$n^0=\beta^{1/2}/(2+\beta^{1/2}),\quad n^+=n^-=1/(2+\beta^{1/2})\ . \tag{A11}$$

2. Case II: Strong illumination ($n,p\gg N_r$)

In this case the neutrality condition (A7) can only be satisfied if $n\approx p$. The equalization between n and p is a consequence of the bimolecular terms $A_t p$ and $A_t n$ in (A2) and (A6), which will shunt the recombination traffic through the dangling bonds for high enough illumination intensities. In this case the steady-state values for n^+, n^0, and n^- can be calculated directly from Eqs. (A1), (A3), and (A5), since $n/p\approx 1$ is now known. One easily obtains

$$\begin{aligned} n^0&=[1+(A^0_n/A^-_p)+(A^0_p/A^+_n)]^{-1}\ ,\\ n^+&=(A^0_p/A^+_n)n^0\ ,\\ n^-&=(A^0_n/A^-_p)n^0\ . \end{aligned} \tag{A12}$$

The two limiting cases I and II are indicated in Fig. 22 for the transition probabilities listed in Table I.

It is evident that the occupancy of the neutral dangling-bond state remains nearly unaffected by the extreme range of illumination intensities spanned by the discussion above. The dangling-bond system reacts to the increase in excess carriers mainly by a population transfer from the positively charged into the negatively charged state. This reflects the larger capture cross section of the dangling bonds for electrons seen in Table I.

For the present study with spin densities $N_s\geq 10^{16}$ cm^{-3} and generation rates $G\leq 5\times 10^{21}$ $\mathrm{cm}^{-3}\,\mathrm{s}^{-1}$ (intensities ≤ 700 $\mathrm{mW/cm}^2$), an upper limit of $n\leq 3\times 10^{14}$ cm^{-3} and $p\leq 7\times 10^{14}$ cm^{-3} can be obtained from Eqs. (A2) and (A6), using the smallest capture cross sections and neglecting the additional bimolecular recombination channel. This means that case I is a valid approximation throughout this study. This has two important consequences.

First, it is possible to define effective transition probabilities $A_n=A^0_n n^0+A^+_n n^+$ and $A_p=A^0_p n^0+A^-_p n^-$ for electron and hole capture by the dangling bonds as proposed in Sec. III B 1, since the occupancies n^+, n^0, and n^- are independent of illumination intensity and time. Using Table I, we obtain $A_n\approx 2.7\times 10^{-9}$ $\mathrm{cm}^3\,\mathrm{s}^{-1}$ and $A_p\approx 0.8\times 10^{-9}$ $\mathrm{cm}^3\,\mathrm{s}^{-1}$.

Secondly, the constancy of n^0 means that under any conditions the room-temperature spin density $N_s=N^0$, as determined by ESR, is a reliable measure for the total dangling-bond density N_r. The discussion above might also explain why at higher temperatures the ESR spin density in undoped amorphous silicon has been found to be unchanged by illumination (missing light-induced ESR of the dangling bonds).

[1]For an overview, see *Amorphous Solids: Low Temperatures Properties,* edited by W. A. Phillips (Springer, Berlin, 1981).

[2]D. E. Graebner, B. Golding, L. C. Allen, J. C. Knights, and D. K. Biegelsen, Phys. Rev. B **29**, 3744 (1984).

[3]M. Stutzmann and D. K. Biegelsen, Phys. Rev. B **28**, 6256 (1983).

[4]D. L. Staebler and C. R. Wronski, Appl. Phys. Lett. **31**, 292 (1977).

[5]N. B. Goodman, Philos. Mag. B **45**, 407 (1982).

[6]M. Grünewald, K. Weber, W. Fuhs, and P. Thomas, J. Phys. (Paris) Colloq. **42**, C4-523 (1981).

[7]D. V. Lang, J. D. Cohen, J. P. Harbison, and A. M. Sergent, Appl. Phys. Lett. **40**, 474 (1982).

[8]J. I. Pankove and J. E. Berkeyheiser, Appl. Phys. Lett. **37**, 705 (1980).

[9]N. M. Amer, A. Skumanich, and W. B. Jackson, Physica (Utrecht) **117&118B**, 897 (1983).

[10]I. Hirabayashi, K. Morigaki, and S. Nitta, Jpn. J. Appl. Phys. **19**, L357 (1980).

[11]H. Dersch, J. Stuke, and J. Beichler, Appl. Phys. Lett. **38**, 456 (1980).

[12]W. Fuhs, M. Milleville, and J. Stuke, Phys. Status Solidi B **89**, 495 (1978).

[13]D. L. Staebler and C. R. Wronski, J. Appl. Phys. **51**, 3262 (1980).

[14]D. Jousse, P. Viktorovitch, L. Vieux-Rochaz, and A. Chenevas-Paul, J. Non-Cryst. Solids **35-36**, 767 (1980).

[15]D. Jousse, R. Basset, S. Delionibus, and B. Bourdon, Appl. Phys. Lett. **37**, 208 (1980).

[16]J. Dresner, D. J. Szostak, and B. Goldstein, Appl. Phys. Lett. **38**, 998 (1981).

[17]I. Sakata, Y. Hayashi, M. Yamanaka, and H. Karasawa, Solid State Electron. **25**, 1059 (1982).

[18]R. A. Street, Appl. Phys. Lett. **42**, 507 (1983).

[19]D. Han and H. Fritzsche, J. Non-Cryst. Solids **59-60**, 397 (1983).

[20]C. R. Wronski, J. Non-Cryst. Solids **59-60**, 401 (1983).

[21]M. Yamaguchi, J. Non-Cryst. Solids **59-60**, 425 (1983).

[22]K. Morigaki, I. Hirabayashi, M. Nakayama, S. Nitta, and K. Shimakawa, Solid State Commun. **33**, 851 (1980).

[23]J. Shah and A. E. DiGiovanni, Solid State Commun. **37**, 153 (1981).

[24]S. Komuro, Y. Aoyagi, Y. Segawa, S. Namba, A. Masuyama, H. Okamoto, and Y. Hamakawa, Appl. Phys. Lett. **42**, 79 (1982).

[25]I. Hirabayashi and K. Morigaki, J. Non-Cryst. Solids **59-60**, 433 (1983).

[26]I. Solomon, T. Dietl, and D. Kaplan, J. Phys. (Paris) **39**, 1241 (1978).

[27]H. Fritzsche, Solar Energy Mater. **3**, 447 (1980).

[28]M. G. Hack and W. I. Milne, Thin Solid Films **76**, 195 (1981).

[29]M. G. Hack and A. Madan, Appl. Phys. Lett. **41**, 272 (1982).

[30]H. Kakinuma, S. Nishikawa, and T. Watanabe, J. Non-Cryst. Solids **59-60**, 421 (1983).
[31]S. Kumar and S. C. Agarwal, Philos. Mag. B **49**, L53 (1984).
[32]D. L. Staebler, R. S. Crandall, and R. Williams, Appl. Phys. Lett. **39**, 733 (1981).
[33]S. Guha, J. Yang, W. Gzubatyj, S. J. Hudgens, and M. Hack, Appl. Phys. Lett. **42**, 589 (1983).
[34]I. Sakata, Y. Hayashi, H. Karasawa and M. Yamanaka, Solid State Commun. **45**, 1055 (1983).
[35]H. Pfleiderer, W. Kusian, and W. Krühler, Solid State Commun. **49**, 493 (1984).
[36]W. Krühler, H. Pfleiderer, R. Plättner, and W. Stetter, in *Optical Effects in Amorphous Semiconductors (Snowbird, Utah, 1984),* edited by P. C. Taylor and S. G. Bishop (AIP, New York, 1984), p. 311 (AIP Conf. Proc. No. 120).
[37]S. R. Elliott, Philos. Mag. B **39**, 349 (1979).
[38]D. Adler, J. Phys. (Paris) Colloq. **42**, C4-3 (1981).
[39]D. Adler, M. E. Eberhart, K. H. Johnson, and S. A. Zygmunt, J. Non-Cryst. Solids **66**, 273 (1984).
[40]M. Wautelet, R. Andrew, M. Failly-Lovato, and L. D. Laude, J. Phys. (Paris) Colloq. **42**, C4-395 (1981).
[41]R. S. Crandall, Phys. Rev. B **24**, 7457 (1981).
[42]R. S. Crandall, D. E. Carlson, A. Catalano, and H. A. Weakliem, Appl. Phys. Lett. **44**, 200 (1984).
[43]N. Nakamura, S. Tsuda, T. Takahama, M. Nishikuni, K. Watanabe, M. Ohnishi, and Y. Kuwano, in *Optical Effects in Amorphous Semiconductors (Snowbird, Utah, 1984),* Ref. 36, p. 303.
[44]D. E. Carlson, A. Catalano, R. V. D'Aiello, C. R. Dickson, and R. S. Oswald, in *Optical Effects in Amorphous Semiconductors (Snowbird, Utah, 1984),* Ref. 36, p. 234.
[45]M. H. Tanielian, N. B. Goodman, and H. Fritzsche, J. Phys. (Paris) Colloq. **42**, C4-375 (1981).
[46]H. Okushi, M. Miyagawa, Y. Tokumaru, S. Yamasaki, H. Oheda, and K. Tanaka, Appl. Phys. Lett. **42**, 895 (1983).
[47]H. Mell and W. Beyer, J. Non-Cryst. Solids **59-60**, 405 (1983).
[48]N. M. Amer, A. Skumanich, and W. B. Jackson, J. Non-Cryst. Solids **59-60**, 409 (1983).
[49]C. Lee and W. Paul (unpublished).
[50]C. C. Tsai, J. C. Knights, R. A. Lujan, B. Wacker, B. L. Stafford, and M. J. Thompson, J. Non-Cryst. Solids **59-60**, 731 (1983).
[51]C. C. Tsai, M. Stutzmann, and W. B. Jackson, in *Optical Effects in Amorphous Semiconductors (Snowbird, Utah, 1984),* Ref. 36, p. 242.
[52]C. C. Tsai, J. C. Knights, and M. J. Thompson, J. Non-Cryst. Solids **66**, 45 (1984).
[53]I. Solomon and M. H. Brodsky, J. Appl. Phys. **51**, 4548 (1980).
[54]S. Hasegawa and Y. Imai, Philos. Mag. B **46**, 239 (1982).
[55]W. B. Jackson, D. K. Biegelsen, R. J. Nemanich, and J. C. Knights, Appl. Phys. Lett. **42**, 105 (1983).
[56]G. Müller, G. Winterling, S. Kalbitzer, and M. Reinelt, J. Non-Cryst. Solids **59-60**, 469 (1983).
[57]R. A. Street, M. J. Thompson, and N. M. Johnson, Philos. Mag. B **51**, 1 (1985).
[58]P. Paduschek, Ch. Höpfl, and H. Mitlehner, Thin Solid Films **110**, 291 (1983).
[59]J. P. Harbison, A. J. Williams, and D. V. Lang, J. Appl. Phys. **55**, 946 (1984).
[60]C. L. Kuo, P. E. Vanier, and J. C. Bilello, J. Appl. Phys. **55**, 375 (1984).
[61]S. Nitta, Y. Takahashi, and M. Noda, J. Phys. (Paris) Colloq. **42**, C4-403 (1981).
[62]N. Nakamura, K. Watanabe, M. Nishikumi, Y. Hishikawa, S. Tsuda, H. Nishikawa, M. Ohnishi, and Y. Kuwano, J. Non-Cryst. Solids **59-60**, 1139 (1983).
[63]H. Dersch, Ph.D. thesis, University of Marburg, 1983 (unpublished).
[64]C. Lee, W. D. Ohlsen, P. C. Taylor, H. S. Ullal, and G. P. Ceasar, in *Optical Effects in Amorphous Semiconductors (Snowbird, Utah, 1984),* Ref. 36, p. 205.
[65]M. Stutzmann, C. C. Tsai, and W. B. Jackson, in *Proceedings of the Conference of the Materials Research Society of Europe, Strasbourg (1984),* edited by P. Pinard and S. Kalbitzer (les éditions physique, Les Ulis, 1984), p. 671.
[66]M. Stutzmann, W. B. Jackson, and C. C. Tsai, Appl. Phys. Lett. **45**, 1075 (1984).
[67]R. A. Street, Adv. Phys. **30**, 593 (1981).
[68]R. A. Street, Phys. Rev. B **26**, 3588 (1982).
[69]F. Boulitrop, Phys. Rev. B **28**, 6192 (1983).
[70]H. Dersch, L. Schweitzer, and J. Stuke, Phys. Rev. B **28**, 4678 (1983).
[71]D. K. Biegelsen, R. A. Street, and R. L. Weisfield, J. Non-Cryst. Solids **66**, 139 (1984).
[72]B. A. Wilson, A. M. Sergent, and J. P. Harbison, Phys. Rev. B **30**, 2282 (1984).
[73]R. A. Street, Philos. Mag. B **49**, L15 (1984).
[74]W. E. Spear, R. J. Loveland, and A. Al-Sharbaty, J. Non-Cryst. Solids **15**, 410 (1974).
[75]C. R. Wronski and R. E. Daniel, Phys. Rev. B **23**, 794 (1981).
[76]B. Hoheisel, R. Fischer, and J. Stuke, J. Phys. (Paris) Colloq. **42**, C4-819 (1981).
[77]W. B. Jackson and M. J. Thompson, Physica (Utrecht) **117&118B**, 883 (1983).
[78]J. Jang, T. M. Kim, J. K. Hyun, J. H. Yoon, and C. Lee, J. Non-Cryst. Solids **59-60**, 429 (1983).
[79]S. Guha, C. Y. Huang, and S. J. Hudgens, Appl. Phys. Lett. **45**, 50 (1984).
[80]D. Wagner and P. Irsigler, Appl. Phys. A **35**, 9 (1984).
[81]It should be mentioned that the assumption of a thermally activated decay constant ν for the annealing process does not follow rigorously from the experimental data because of the narrow useful temperature range. We cannot exclude alternative explanations for the observed temperature dependence.
[82]R. A. Street, Philos. Mag. B **37**, 35 (1978).
[83]R. A. Street, J. Zesch, and M. J. Thompson, Appl. Phys. Lett. **43**, 672 (1983).
[84]M. Stutzmann and J. Stuke, Solid State Commun. **47**, 635 (1983).
[85]A. Skumanich and N. Amer, J. Non-Cryst. Solids **59-60**, 249 (1983).
[86]M. Stutzmann (unpublished).
[87]M. Janai and M. Stutzmann, Phys. Status Solidi B (to be published).
[88]W. Beyer and H. Wagner, J. Appl. Phys. **53**, 8745 (1982).
[89]K. Zellama, P. Germain, S. Squelard, J. Monge, and E. Ligeon, J. Non-Cryst. Solids **35-36**, 225 (1980).
[90]R. Bachus, B. Movaghar, L. Schweitzer, and U. Voget-Grote, Philos. Mag. B **39**, 27 (1979).
[91]W. M. Pontuschka, W. W. Carlos, P. C. Taylor, and R. W. Griffith, Phys. Rev. B **25**, 4362 (1982).
[92]D. K. Biegelsen, R. A. Street, C. C. Tsai, and J. C. Knights, Phys. Rev. B **20**, 4839 (1979).
[93]H. v. Löhneysen, J. H. Schink and W. Beyer, Phys. Rev. Lett. **52**, 549 (1984).
[94]J. E. Graebner, B. Golding, L. C. Allen, D. K. Biegelsen, and M. Stutzmann, Phys. Rev. Lett. **52**, 553 (1984).
[95]Y. J. Chabal and C. K. N. Patel, Phys. Rev. Lett. **53**, 210

(1984).
[96]J. B. Boyce and M. Stutzmann, Phys. Rev. Lett. **54**, 562 (1985).
[97]W. Fuhs, in *Festkörperprobleme (Advances in Solid State Physics)*, edited by P. Grosse (Pergamon/Vieweg, Braunschweig, 1984), Vol. XXIV, p. 133.
[98]H. Schade, in *Semiconductors and Semimetals,* edited by J. I. Pankove (Academic, New York, 1984), Vol. 21B, p. 359.
[99]R. A. Street, D. K. Biegelsen, and J. C. Knights, Phys. Rev. B **24**, 969 (1981).
[100]W. den Boer, M. J. Geerts, M. Ondris, and H. M. Wentinck, J. Non-Cryst. Solids **66**, 363 (1984).